

Antenna Selection for Reconfigurable Intelligent Surfaces: A Transceiver-Agnostic Passive Beamforming Configuration

Chao Xu, *Senior Member, IEEE*, Jiancheng An, *Member, IEEE*, Tong Bai, *Member, IEEE*, Shinya Sugiura, *Senior Member, IEEE*, Robert G. Maunder, *Senior Member, IEEE*, Lie-Liang Yang, *Fellow, IEEE* Marco Di Renzo, *Fellow, IEEE* and Lajos Hanzo* *Life Fellow, IEEE*

Abstract—Reconfigurable intelligent surface (RIS) is capable of improving the wireless system performance by steering the reflected signal in the desired direction. One of the major challenges is that both the transceiver and RIS have to be jointly optimized, where the optimization problems have to be reformulated for different system models and scenarios. To circumvent this challenge, new low-complexity antenna selection (AS) algorithms for transceiver-agnostic RIS configuration are proposed. Given a multiple-input multiple-output (MIMO) channel, the proposed RIS-AS opts for accurately aligning the RIS both with the transmit antenna (TA) and receive antenna (RA) for the sake of maximizing the MIMO channel’s overall output power. The proposed RIS-AS only has to configure the RIS alone, i.e. without iterations with the transceiver optimization. As a result, the proposed RIS-AS has the compelling benefit that they are generically applicable, regardless of the specific transceiver architecture. Our simulation results confirm that the proposed RIS-AS is capable of supporting any MIMO configuration, regardless of their closed/open-loop, single-/full-RF and multiplexing-/diversity-oriented setups.

Index Terms—Reconfigurable intelligent surface, passive beamforming, active beamforming, antenna selection, index modulation, spatial modulation, single-RF, full-RF, space-time shift keying, multiplexing, diversity.

I. INTRODUCTION

A. The State-of-the-Arts

The recent developments in reconfigurable intelligent surfaces (RIS) [1]–[3] have inspired the revolutionary notion of smart radio environments. More explicitly, the RIS consists of a dense population of near-passive elements, which reflect the signal in the desired direction without using radio-frequency (RF) chains. There has been an upsurge of interest in the

passive beamforming capability of RISs, where the phase rotations of the direct and reflected links are accurately aligned, so that the received signals are constructively superimposed at the desired user and cancelled at the non-intended users. The RIS-based passive beamforming is a direct descendant of reflectarrays that are widely used both in radar and in satellite communications. However, in contrast to a reflectarray fabricated with a prescribed radiation pattern, the RIS has the benefit of real-time reconfigurability and control, rendering them practically appealing for high-dynamic wireless applications. *The major challenge* is now that the transceiver parameters and RIS parameters have to be jointly optimized, which is nontrivial under the nonconvex constraints imposed by the RIS operating without RF chains. To elaborate, both RIS-assisted single-input single-output (SISO) and multi-user multiple-input single-output (MU-MISO) schemes were proposed in [4], where the NP-hard problem of optimizing both the transmit beamforming vector and the RIS configuration was approximated by the suboptimal semidefinite relaxation (SDR) and alternating optimization (AO) solutions. Alternatively, both manifold optimization [5] and deep learning [6] were conceived for the signal-to-noise ratio (SNR) maximization problem of RIS assisted MISO systems. As a further advance, RISs were also integrated into multiple-input multiple-output (MIMO) systems in [7], where the AO algorithm was conceived for optimizing both the transmit covariance matrix and the RIS coefficients. Moreover, due to the lack of baseband processing capabilities at the RIS, the same set of RIS coefficients has to be applied to different subcarriers in orthogonal frequency-division multiplexing (OFDM). In order to alleviate this problem, a successive convex approximation (SCA) technique was conceived in [8], while the authors of [9] opted for aligning the RIS to the strongest time-domain path. Furthermore, RIS optimization in the face of hardware impairments - including phase noise, quantization errors, amplifier non-linearity and spatial correlation - was investigated in [10]–[13]. Moreover, the RIS has also been optimized for a variety of objectives, including the symbol error rate [14] and energy-efficiency [15]. Finally, the optimization of RIS passive beamforming has been extensively studied in a variety of wireless scenarios, including the weighted sum rate maximization of multi-cell and cell-free MIMO systems [16], [17], the power minimization of non-orthogonal multiple access (NOMA) [18], [19], the latency minimization of mobile edge computing [20], [21], the joint optimization of simultaneous wireless information and power transfer (SWIPT) [22], [23] and the secrecy rate maximization

C. Xu, R. G. Maunder L.-L. Yang and L. Hanzo are with the School of Electronics and Computer Science, University of Southampton, Southampton SO17 1BJ, UK (e-mail: {cx1g08,rm,lly,lh}@soton.ac.uk). J. An is with the Engineering Product Development Pillar, Singapore University of Technology and Design, Singapore 487372 (e-mail: jiancheng_an@163.com). S. Sugiura is with the Institute of Industrial Science, University of Tokyo, Meguro-ku, Tokyo 153-8505, Japan (e-mail: sugiura@ieee.org). M. Di Renzo is with Université Paris-Saclay, CNRS, CentraleSupélec, Laboratoire des Signaux et Systèmes, 3 Rue Joliot-Curie, 91192 Gif-sur-Yvette, France. (marco.direnzo@universite-paris-saclay.fr).

The work of T. Bai was supported in part by NSFC China under Project 62101015. The work of S. Sugiura was supported in part by National Institute of Information and Communications Technology (NICT), Japan. The work of M. Di Renzo was supported in part by the European Commission through the H2020 ARIADNE project under grant agreement number 871464 and through the H2020 RISE-6G project under grant agreement number 101017011. L. Hanzo would like to acknowledge the financial support of the Engineering and Physical Sciences Research Council projects EP/W016605/1 and EP/X01228X/1 as well as of the European Research Council’s Advanced Fellow Grant QuantCom (Grant No. 789028).

in physical layer security [24], [25].

In addition to improving the radio environments, RIS is also capable of performing intelligent *reflection-based modulation*, where extra information is embedded in the reflection pattern [26]. Due to their similarities, the RIS reflection-based modulation is illustrated here by analogy with its close relative of backscatter communication [27]. First of all, similar to bistatic backscatter radio, a separate RF source generates a carrier signal without any user data, where both the amplitude and phase of each RIS element represents a PSK/QAM symbol mapped onto the impinging radio wave [28]–[32]. This is especially beneficial for reducing the transmitter’s hardware cost in the millimeter-wave and terahertz bands. Furthermore, RISs can also be invoked for performing frequency up/down-conversion by linearly changing the RIS phases with time, allowing the analog and RF circuits to operate at a relatively low frequency [29]. Secondly, ambient backscatter radio is known to map its symbols onto ambient sources such as TV signals or Wi-Fi signals that carry their own primary information. Inspired by this, the joint modulation of the transmitted signals and the RIS responses was proposed in [33], where the RIS had a sufficiently degree of freedom to map a PSK symbol onto the reflection of the impinging modulated signals. In [31], [34], the symbols mapped onto the RIS responses form a MIMO codebook that is independent from the signal modulation at the transmitter. Furthermore, the joint mapping of the transmitted signal and of the RIS patterns is optimized for minimizing the bit error rate (BER) in [35]. Thirdly, the backscatter load modulation switches between the absorbing and reflecting states, which represent a modulated bit of ‘0’ and ‘1’, respectively. This is in line with the principle of index modulation (IM) [36], [37], where the specific activation pattern conveys extra bits. Following this philosophy, a subset of M_A out of M RIS elements are activated for carrying out passive beamforming in [38], [39], where the specific activation index is controlled by $\lfloor \log_2 \binom{M}{M_A} \rfloor$ IM bits. Furthermore, the RIS assisted spatial modulation (SM) is conceived in [40]–[44], where the RIS is accurately aligned with a pair of transmit antenna (TA) and receive antenna (RA), which conveys IM bits in the spatial-domain. Finally, it is of paramount importance to note that despite their similarities, the major difference between RIS and backscatter is that in addition to reflection-based modulation, the RIS also facilitates passive beamforming either by explicitly maximizing the SNR or by implicitly minimizing the BER.

The state-of-the-art RIS schemes are summarized in Table I. The closed-loop systems require a feedback link in order to make the receiver’s channel state information (CSI) available at the transmitter (CSI-T). By contrast, the open-loop systems assume that CSI is only available at the receiver (CSI-R). It can be seen in Table I that most existing RIS schemes require CSI-T in order to jointly optimize transmitted signalling and RIS configuration. The exceptions are [29], [33], where the RISs modulate symbols purely based on their own data streams.

B. Major Challenges and Open Problems

The major challenges of RIS-aided passive beamforming include the following aspects. First of all, the AO methods [4],

[7], [10], [12], [47] generally have polynomial complexity as a function of N_T , N_R and M [3], which represent the number of TAs, that of RAs and that of RIS elements, respectively. Considering the family of RIS assisted MIMO systems, the AO of [7] invokes singular decomposition (SVD) once, matrix inversion M times and eigenvalue decomposition (EVD) $(M + 1)$ times in each iteration. This excessive complexity encumbers the realistic deployability of RIS. Secondly, it can be readily seen in Table I that the optimization problem and its solution methods have to be reformulated for different system models and scenarios, which impedes our “plug-and-play” goal. Thirdly, the high-mobility scenarios are envisioned to be of crucial importance [48]–[50]. However, when the fading fluctuates over time, the high-complexity AO algorithms that involve matrix inversions and EVDs have to be frequently repeated based on the updated CSI, which may become impractical in the much-anticipated space-air-ground integrated networks (SAGIN) [51]–[55].

On a similar note, the major challenges of RIS reflection-based modulation are also three-fold. First of all, the specific mapping of bits to transmit signals and RIS patterns [34], [35], [38], [39] is of crucial importance. If the mapping codebook is established at the transmitter, a lossless control link that carries a substantial portion of the system throughput for modulating the RIS is required between the transmitter and the RIS [29]–[35], [38]–[44]. This is extremely challenging in practice, bearing in mind that the RIS does not have error correction capability. Secondly, even if the bits are mapped to the transmitted signals and RIS patterns separately, the concurrent signal transmission of the two information sources leads to either high-complexity joint detection at the receiver or to error propagation from separate detection. Thirdly, although RIS reflection-based modulation may achieve a higher throughput than RIS passive beamforming, the former inevitably suffers from a reduced received signal power compared to the latter [33], [35], [38], [39], due to the fact that the RIS beamforming capability is sacrificed for modulating signals at RIS. Bearing in mind that the signal modulating capability of RIS operating without RF chains is inferior to that of RF-powered transmitters, a fair comparison between RIS passive beamforming and RIS reflection-based modulation should be carried out under the same overall throughput instead of using the same number of modulation levels, which is often overlooked.

Against this background, the following key questions arise:

- (Q-1) **Beamforming versus modulation:** Given the same hardware cost and throughput, which one is better between RIS passive beamforming and RIS reflection-based modulation?
- (Q-2) **Complexity and adaptivity:** How can we reduce the RIS configuration complexity, so that it may become easier to adapt to the dynamic wireless environment?
- (Q-3) **Independency and deployability:** Is it possible to make the RIS configuration independent of the transceiver architecture, so that the off-the-shelf RIS can be deployed as a “plug-and-play” add-on for different wireless systems?

TABLE I: State-of-the-arts of RIS passive beamforming and reflection-based modulation schemes.

	System model	Passive beamforming			Reflection-based modulation			Further improvements
		Parameters	Objectives	Methods	Transmitter	RIS	Receiver	
Wu <i>et al.</i> [4]	Closed-loop MU-MISO downlink	Transmitter beamforming and RIS	Power maximization	SDR, AO				[5] invoked manifold optimization; [6] conceived deep reinforcement learning.
Zhang <i>et al.</i> [7]	Closed-loop MIMO	Transmitter beamforming and RIS	Capacity maximization	AO				[8] proposed successive convex approximation; [9] aligned RIS to the strongest path.
Ye <i>et al.</i> [14]	Closed-loop MIMO	Transmitter beamforming and RIS	Symbol error rate minimization	AO				[45] proposed SER minimization in MU-MISO.
Huang <i>et al.</i> [15]	Closed-loop MU-MISO downlink	Transmitter beamforming and RIS	Energy efficiency maximization	AO				[46] deployed multiple RISs; [47] extends to device-to-device communication scenarios.
Wu <i>et al.</i> [10]	Closed-loop MU-MISO downlink	Transmitter beamforming, discrete RIS	Power maximization	AO				[11] investigated quantization levels; [12] extended the study to hardware impairments.
Proposed scheme	Generic MIMO	RIS configuration	Power maximization	Antenna selection				
Tang <i>et al.</i> [29]	Open-loop SISO				Generate unmodulated RF signal	Modulate a PSK	Another RIS for down-conversion	[30] extended to modulating MIMO QAM at RIS.
Basar <i>et al.</i> [32]	Closed-loop SISO			RIS aligned to a TA-RA pair	Generate unmodulated RF signal	Modulate a PSK		[31] modulated Alamouti's G2 at RIS.
Karasik <i>et al.</i> [33]	Open-loop SIMO				Generate modulated signal	Modulate PSK symbols		[34] modulated MIMO signals at RIS; [35] jointly optimized the mapping of transmitted signal and RIS patterns.
Yan <i>et al.</i> [38]	Closed-loop MU-MISO downlink	RIS activation and configuration	Capacity maximization	majorization-minimization	Modulate V-BLAST	IM by RIS activation		[39] added transmitter beamforming and fixed the number of activated RIS elements.
Basar [40]	Closed-loop SIMO			RIS aligned to a TA-RA pair	Generate modulated signal	RSM by aligning RIS to a RA	A single RA has maximized power	[41] extended to multiple RAs; [42] extended SM to TA; [43] proposed quadrature SM; [44] extended SM to both TA & RA.

C. Novel Contributions

Against this background, we propose new antenna selection (AS) algorithms in order to facilitate transceiver-agnostic RIS passive beamforming. The conventional joint transceiver-RIS optimization schemes not only impose substantially increased computational complexity in the physical (PHY) layer, but they also require modifications in the medium access control (MAC) layer's configuration and beam management protocols [56], [57]. By contrast, given a MIMO channel, the proposed RIS-AS opts for accurately aligning the RIS with a pair of TA and RA for the sake of maximizing the channel's output power. The proposed RIS-AS only has to **configure the RIS alone, i.e. without iterations with the transceiver optimization**, which is agnostic to the specific choices of the PHY transceivers and MAC protocols. As a benefit of our transceiver-agnostic RIS configuration, the proposed RIS-AS is capable of supporting any MIMO transmission, regardless of their closed/open-loop, single-/full-RF and multiplexing-/diversity-oriented setups. The novel contributions of this work are summarized as follows:

- We propose three RIS-AS algorithms: (I) all RIS elements are aligned to the TA-RA pair that is associated with the highest channel power in the direct link; (II) all RIS elements are aligned to the TA-RA pair that results in the highest power for the composite RIS aided SIMO/MISO/MIMO channel; (III) each RIS element has the degree of freedom to be aligned to a pair of TA and RA, so that the overall output power of the composite RIS aided SIMO/MISO/MIMO channel is maximized. The generic far-field RIS communication model of [58]–[60] is considered, where the fading channels vary over time according to the Doppler frequency [51]–[54].

- In answer to **(Q-1)**, the performance of RIS-AS aided passive beamforming and that of RIS-SM [40]–[44] for reflection-based modulation are compared under the same throughput. Our performance analysis and simulation results demonstrate that owing to the fact that the RIS beamforming capability is sacrificed for conveying IM bits in RIS-SM, the proposed RIS-AS is capable of achieving substantial performance advantages.
- With regard to **(Q-2)**, compared to the AO algorithms of [4], [7], [10], [12], [47] that iteratively optimize the transmitter's beamforming weights and the RIS patterns, the proposed RIS-AS algorithms only have to check the channel's output power associated with different TA-RA pairs. Our simulation results demonstrate that the RIS-AS configuration conceived for closed-loop MIMO beamforming is capable of approaching the performance of AO optimization, despite its substantially lower complexity.
- As to **(Q-3)**, the RIS-AS is designed to be independent of the transceiver structure, where any MIMO transmission can be supported. In order to demonstrate this, we present performance results for a variety of MIMO transceivers that only assume CSI-R, including the full-RF V-BLAST and generalized space-time shift keying (GSTSK) [61]–[63], as well as the single-RF SM and STSK [64]–[66]. Our simulation results demonstrate that RIS-AS is capable of improving the performance of any MIMO schemes, regardless of whether they have closed/open-loop, single-/full-RF and multiplexing-/diversity-oriented setups.

We note that this work is different from the joint AS and RIS designs of [67]–[70]. The RIS-AS proposed in this paper is dedicated to the RIS configuration that is independent of the transceiver architecture, while the authors of [67]–[70] applied

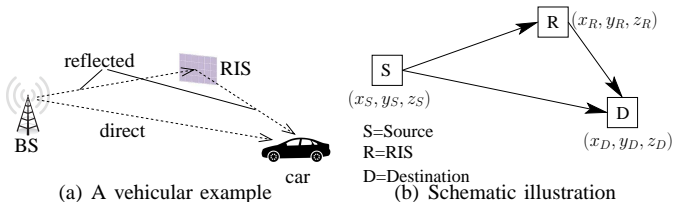


Fig. 1: RIS assisted high-mobility wireless communication systems.

the AS philosophy to transmitter beamforming. Specifically, when the number of RF chains is lower than the number of antennas at the transmitter, the AS-based beamforming constitutes an energy-efficient alternative to hybrid beamforming, where a subset of TAs is physically switched off at the transmitter. Considering that the waterfilling-based eigenmode transmission achieves the optimal performance, in this paper, we opt for using digital beamforming transceivers for the closed-loop MIMO scenarios.

D. Organization and Notations

This paper is organized as follows. The system model is presented in Sec. II. The RIS-AS algorithms for assisting open-loop SIMO and closed-loop MISO are proposed in Secs. III and IV, respectively, which are extended from the closed-form RIS optimization for SISO. These solutions are further generalized to the closed-loop MIMO and open-loop MIMO in Secs. V and VI, respectively. The impacts of RIS channel estimation are discussed in Sec. VII. Finally, our conclusions are offered in Sec. VIII.

The following notations are used throughout the paper. The operations $(\cdot)^*$ and $(\cdot)^H$ denote the conjugate of a complex number and the Hermitian transpose of a complex matrix, respectively. The notations $\ln(\cdot)$ and $\exp(\cdot)$ refer to natural logarithm and natural exponential functions, respectively. The notations $p(\cdot)$ and $E(\cdot)$ represent the probability and the expectation, respectively. $\mathbf{a} \in \mathcal{C}^{N \times 1}$ refers to a complex-valued vector of size $(N \times 1)$, and $\mathbf{A} \in \mathcal{C}^{c \times d}$ denotes that \mathbf{A} is a complex-valued matrix of size $(c \times d)$.

II. SYSTEM MODEL

A. General Setups

Fig. 1 exemplifies a vehicular communication scenario assumed in this paper, where the coverage of a high-mobility user is enhanced by a RIS. Nonetheless, three-dimensional representation of the source-destination (SD) link, source-RIS (SR) link and RIS-destination (RD) link conceived in this paper can be readily applied to satellites, airplanes, unmanned aerial vehicles, trains and cars under the SAGIN framework [48]–[55], because the mobilities of the source, RIS and destination are all taken into account in our system model.

The source node (transmitter) and the destination node (receiver) are equipped with N_T and N_R antennas, respectively, where a uniform linear array (ULA) is deployed at both sides. The RIS is assumed to be comprised of M passive reflecting elements, where a uniform planar array (UPA) is adopted. The RIS reflection coefficients at the n -th time slot are denoted as $\alpha_n = [\alpha_n^1, \dots, \alpha_n^M]^T$, where $\{|\alpha_n^m| = 1\}_{m=1}^M$ are optimized by maximizing the signal power received at the destination.

The RIS is configured with the aid of a smart controller using field-programmable gate array (FPGA) circuits. For the closed-loop and open-loop MIMO transceiver architectures, the RIS parameters are evaluated at the transmitter based on CSI-T and at the receiver based on CSI-R, respectively. This control information can be conveyed by a separate link such as bluetooth, and the associated time duration has negligible impact on the data rate compared to the pilot overhead, as assumed in [8], [9], [71]–[73].

B. Large-Scale Fading

The path loss (PL) of each link is given by [50], [74]–[79]:

$$PL = -10\gamma \log_{10}(d) - 20 \log_{10} \left(\frac{4\pi}{\lambda} \right) + G_e = 10 \log_{10} \Gamma \text{ dB}, \quad (1)$$

where γ denotes the PL exponent (PLE). The effective antenna gain is formulated as $(G_e = \frac{4\pi A_e}{\lambda^2})$, where A_e refers to the antenna aperture of the transmitter or the receiver, while f_c and $\lambda = \frac{c}{f_c}$ refer to the carrier frequency and the wavelength, respectively. The distance d is evaluated in real-time based on the coordinates seen in Fig. 1(b). For example, the distance of the SD link is evaluated by $[d^{SD} = \sqrt{(x_S - x_D)^2 + (y_S - y_D)^2 + (z_S - z_D)^2}]$. The non-logarithmic PL is given by Γ , which is updated based on the distance for each sampling period. In summary, the PL of (1) is a function of distance and carrier frequency/wavelength, which allows us to examine the performance of RIS assisted high-mobility systems in different frequency bands. On one hand, based on Friis' Law, the PL component of $[20 \log_{10}(4\pi/\lambda)]$ increases quadratically with f_c . On the other hand, the antenna apertures of the source and destination nodes, namely A_e^S and A_e^D , shrink as f_c increases. As a result, given fixed antenna sizes, the effective antenna gains of the source and destination nodes G_e^S and G_e^D also increase quadratically with f_c . More details on these relationships can be found in [50], [78], [79]. Moreover, assuming the same PLE for the SR and RD links as $\gamma^{SRD} = \gamma^{SR} = \gamma^{RD}$, the overall PL of the cascaded source-RIS-destination is given by $\Gamma^{SRD} = \Gamma^{SR} \Gamma^{RD} \propto \frac{1}{(d^{SR} d^{RD})^{\gamma^{SRD}}}$. This implies that under generic far-field conditions, the RIS-reflected links suffer from severe PL that is inversely proportional to the product of the segment distances. In this paper, we will thoroughly investigate the effects of different PLEs, operating frequencies and distances on the link budget and performance evaluation.

C. Small-Scale Fading

This paper investigates time-varying flat Ricean fading channels, which take into account both line-of-sight (LoS) and non-LoS (NLoS). Let us consider a system having 100 kHz of bandwidth centered at $f_c = 2.6\text{GHz}$ in the S-band [50], which is sufficient for high-mobility Command & Control (C&C) link coverage [53]. On one hand, if the user moves at 90 mph, the coherence time over which the time correlation function is higher than 0.5 is estimated to cover only 51 symbols, hence time-varying fading directly governed by the Doppler frequency is modelled in this paper. On the other hand, for the ease of illustration, we assume that the distance between the BS and the user is on the order of hundreds of meters, which is substantially lower than c/f_s , where c and f_s are the

speed of light and symbol rate, respectively. This implies that the delay-spread of the multipath components including those reflected by RIS does not exceed the symbol-level sampling period, hence justifying the narrowband system assumption. In summary, the high-mobility small-scale Ricean fading of each link - including the SD, SR and RD links - is modelled by: [52], [80]–[82]

$$h_n = h_n^{\text{LoS}} + h_n^{\text{NLoS}} = \sqrt{\frac{K}{1+K}} \exp(j2\pi n \Delta f^{\text{LoS}}) + h_n^{\text{NLoS}}. \quad (2)$$

Both the LoS and NLoS components of (2) vary for each symbol index n . The LoS component of (2) is given by $h_n^{\text{LoS}} = \sqrt{\frac{K}{1+K}} \exp(j2\pi n \Delta f^{\text{LoS}})$, where the Ricean K-factor determines the power ratio between the LoS and the NLoS components. The frequency offset of the LoS path is induced by the movement as $\Delta f_n^{\text{LoS}} = f_d \cos(\phi_0)$, where the normalized maximum Doppler frequency is given by $f_d = \frac{vf_c}{c}$, while v represents the vehicle's velocity. As an example, the angle between the LOS and the moving direction is formulated by $\phi_0^{\text{SD}} = \arctan \frac{y_S - y_D}{x_S - x_D}$ for the SD link. Moreover, the NLoS component in (2) is generated by Clarke's model [83], [84] associated with a power of $\frac{1}{1+K}$ as $h_n^{\text{NLoS}} \sim \mathcal{CN}(0, \frac{1}{1+K})$. The correlation over time is given by $E[h_n^{\text{NLoS}}(h_{n'}^{\text{NLoS}})^*] = \frac{1}{1+K} J_0(2\pi f_d |n - n'|)$, where $J_0(\cdot)$ is the Bessel function of the first kind. The detailed fading parameters of the SD, SR and RD links are summarized in Table II.

D. Major Benchmark Schemes

For the closed-loop MIMO relying on CSI-T, the waterfilling-based eigenmode transmission is employed, and the RIS is configured by the transmitter based on CSI-T. The AO methods [4], [7], [10], [12], [47] that jointly optimize the transceiver beamforming weights and RIS patterns constitute important benchmarks. We note that as introduced in Sec. I, the existing RIS optimization approaches also include SCA [8], manifold optimization [5] and deep learning [6], which have not been extended to the MIMO beamforming transceiver. The projected gradient method proposed in [85] is capable of accelerating the AO convergence, but it does not eliminate the AO's matrix inversions and SVD/EVDs in each iteration. It was also demonstrated in [86] that deep learning is capable of outperforming both AO and SDR operating without waterfilling. The interested readers might like to refer to [1]–[3] for detailed RIS optimization approaches.

For the open-loop MIMO with CSI-R, the RIS can be configured by the receiver, which is completely agnostic to the MAC-PHY cross-layer protocols on constellation and beam management. As discussed in Sec. I, most existing RIS schemes require CSI-T for joint optimization. In order to avoid digressing from the main focus, for MIMO schemes without beamforming at the transmitter, the RIS-SM schemes [40]–[44] are compared to the proposed RIS-AS at the same hardware cost and throughput in this paper.

III. AS FOR RIS ASSISTED OPEN-LOOP SIMO WITH CSI-R

A. Received Signal Model

First of all, the Ricean fading for the direct SD link is modelled as $\mathbf{h}_n^{\text{SD}} = \mathbf{h}_n^{\text{SD,LoS}} + \mathbf{h}_n^{\text{SD,NLoS}} \in \mathcal{C}^{N_R \times 1}$, which is associ-

ated with a single TA and N_R RAs. The LoS paths are formulated as $\mathbf{h}_n^{\text{SD,LoS}} = \sqrt{\frac{K^{\text{SD}}}{1+K^{\text{SD}}}} \exp(j2\pi n \Delta f^{\text{SD,LoS}}) \mathbf{a}_{\text{ULA}}(\theta_D^{\text{AoA}})$, where $\theta_D^{\text{AoA}} \in (0, 2\pi]$ denotes the angle-of-arrival (AoA) at the receiver, while the N -element ULA response vector is given by:

$$\mathbf{a}_{\text{ULA}}(\theta) = [1, \dots, \exp(j\frac{2\pi}{\lambda} d \sin \theta), \dots, \exp(j\frac{2\pi}{\lambda} (N-1) d \sin \theta)]^T, \quad (3)$$

where d denotes the inter-element spacing. Furthermore, the r -th element of the NLoS vector $\mathbf{h}_n^{\text{SD,NLoS}}$ is generated by Clarke's model associated with f_d^{SD} and $\mathbf{h}_n^{\text{SD,NLoS},r} \sim \mathcal{CN}(0, \frac{1}{1+K^{\text{SD}}})$ for $(1 \leq r \leq N_R)$, as described in Sec. II-C.

Secondly, the SR link is modelled as $\mathbf{h}_n^{\text{SR}} = \mathbf{h}_n^{\text{SR,LoS}} + \mathbf{h}_n^{\text{SR,NLoS}} \in \mathcal{C}^{M \times 1}$ for the M RIS elements, where the LoS part is given by $\mathbf{h}_n^{\text{SR,LoS}} = \sqrt{\frac{K^{\text{SR}}}{1+K^{\text{SR}}}} \exp(j2\pi n \Delta f^{\text{SR,LoS}}) \mathbf{a}_{\text{UPA}}(\theta_R^{\text{AoA}}, \varphi_R^{\text{AoA}})$, while $\theta_R^{\text{AoA}} \in (0, 2\pi]$ and $\varphi_R^{\text{AoA}} \in (0, 2\pi]$ refer to the azimuth and elevation AoAs, respectively. Moreover, the UPA response vector having $(M = M_y M_z)$ dual-polarized elements is given by:

$$\mathbf{a}_{\text{UPA}}(\theta, \varphi) = [1, \dots, \exp\{j\frac{2\pi}{\lambda} d [m_y \sin \theta \cos \varphi + m_z \sin \varphi]\}, \dots, \exp\{j\frac{2\pi}{\lambda} d [(M_y - 1) \sin \theta \cos \varphi + (M_z - 1) \sin \varphi]\}]^T, \quad (4)$$

where we have $(0 \leq m_y \leq M_y - 1)$ and $(0 \leq m_z \leq M_z - 1)$. The m -th element of the NLoS vector is generated by Clarke's model with f_d^{SR} and $\mathbf{h}_n^{\text{SR,NLoS},m} \sim \mathcal{CN}(0, \frac{1}{1+K^{\text{SR}}})$ for $(1 \leq m \leq M)$.

Thirdly, the RD link is modelled as $\mathbf{H}_n^{\text{RD}} = \mathbf{H}_n^{\text{RD,LoS}} + \mathbf{H}_n^{\text{RD,NLoS}} \in \mathcal{C}^{N_R \times M}$. The LoS matrix is $\mathbf{H}_n^{\text{RD,LoS}} = \sqrt{\frac{K^{\text{RD}}}{1+K^{\text{RD}}}} \exp(j2\pi n \Delta f^{\text{RD,LoS}}) \mathbf{a}_{\text{ULA}}(\theta_D^{\text{AoA}}) \mathbf{a}_{\text{UPA}}(\theta_R^{\text{AoD}}, \varphi_R^{\text{AoD}})^H$, where $\theta_R^{\text{AoD}} \in (0, 2\pi]$ and $\varphi_R^{\text{AoD}} \in (0, 2\pi]$ refer to the azimuth and elevation angle-of-departures (AoDs) from RIS. The element on the r -th row and m -th column of the NLoS matrix $\mathbf{H}_n^{\text{RD,NLoS}}$ is generated by Clarke's model with f_d^{RD} and $\mathbf{H}_n^{\text{RD,NLoS},r,m} \sim \mathcal{CN}(0, \frac{1}{1+K^{\text{RD}}})$ for $(1 \leq r \leq N_R)$ and $(1 \leq m \leq M)$.

Finally, the signals received at the destination from both direct and RIS-reflected links are:

$$\begin{aligned} \mathbf{y}_n &= \mathbf{h}_n s_n + \mathbf{v}_n \\ &= (\mathbf{h}_n^{\text{SD}} + \sum_{m=1}^M \alpha_n^m \mathbf{H}_n^{\text{RD},-m} \mathbf{h}_n^{\text{SR},m}) s_n + \mathbf{v}_n \\ &= (\mathbf{h}_n^{\text{SD}} + \sum_{m=1}^M \alpha_n^m \mathbf{H}_n^{\text{SRD},-m}) s_n + \mathbf{v}_n, \end{aligned} \quad (5)$$

where s_n and $\mathbf{v}_n \in \mathcal{C}^{N_R \times 1}$ are the transmitted signal and the additive white Gaussian noise (AWGN) vector with $\mathbf{v}_n^r \sim \mathcal{CN}(0, N_0)$, respectively, while N_0 is the noise power. The vectors of $\mathbf{H}_n^{\text{RD},-m} \in \mathcal{C}^{N_R \times 1}$ and $\mathbf{H}_n^{\text{SRD},-m} \in \mathcal{C}^{N_R \times 1}$ refer to the m -th column in $\mathbf{H}_n^{\text{RD}} \in \mathcal{C}^{N_R \times M}$ and $\mathbf{H}_n^{\text{SRD}} \in \mathcal{C}^{N_R \times M}$, respectively. We have the equivalent $(\mathbf{h}_n = \mathbf{h}_n^{\text{SD}} + \sum_{m=1}^M \alpha_n^m \mathbf{H}_n^{\text{RD},-m} \mathbf{h}_n^{\text{SR},m})$ and $(\mathbf{H}_n^{\text{SRD},m} = \mathbf{H}_n^{\text{RD},r,m} \mathbf{H}_n^{\text{SR},m})$ in (5), where $\mathbf{H}_n^{\text{SRD},r,m}$ and $\mathbf{H}_n^{\text{RD},r,m}$ refer to the element on the r -th row and m -th column of the matrices $\mathbf{H}_n^{\text{SRD}}$ and \mathbf{H}_n^{RD} , respectively, while $\mathbf{h}_n^{\text{SR},m}$ refers to the m -th element of the vector \mathbf{h}_n^{SR} .

B. Problem Formulation and Antenna Selection Algorithms

The RIS optimization problem is formulated as:

$$\begin{aligned} &\max_{\{\alpha_n^m\}_{m=1}^M} \|\mathbf{h}_n\|^2 \\ &= \max_{\{\alpha_n^m\}_{m=1}^M} \|\mathbf{h}_n^{\text{SD}} + \sum_{m=1}^M \alpha_n^m \mathbf{H}_n^{\text{RD},-m} \mathbf{h}_n^{\text{SR},m}\|^2, \\ &\text{s.t. } \{|\alpha_n^m| = 1\}_{m=1}^M. \end{aligned} \quad (6)$$

TABLE II: Key model parameters of RIS-assisted system.

	Source-Destination (SD) Link	Source-RIS (SR) Link	RIS-Destination (RD) Link
Distance	$d^{\text{SD}} = \sqrt{(x_S - x_D)^2 + (y_S - y_D)^2 + (z_S - z_D)^2}$	$d^{\text{SR}} = \sqrt{(x_S - x_R)^2 + (y_S - y_R)^2 + (z_S - z_R)^2}$	$d^{\text{RD}} = \sqrt{(x_R - x_D)^2 + (y_R - y_D)^2 + (z_R - z_D)^2}$
PL exponent	γ^{SD}	γ^{SR}	γ^{RD}
PL	$\Gamma^{\text{SD}} = (d^{\text{SD}})^{-\gamma^{\text{SD}}} \left(\frac{4\pi}{\lambda}\right)^{-2} 10^{0.1(G_e^{\text{Tx}} + G_e^{\text{Rx}})}$	$\Gamma^{\text{SR}} = (d^{\text{SR}})^{-\gamma^{\text{SR}}} \left(\frac{4\pi}{\lambda}\right)^{-2} 10^{0.1G_e^{\text{Tx}}}$	$\Gamma^{\text{RD}} = (d^{\text{RD}})^{-\gamma^{\text{RD}}} \left(\frac{4\pi}{\lambda}\right)^{-2} 10^{0.1G_e^{\text{Rx}}}$
Ricean factor	K^{SD}	K^{SR}	K^{RD}
LoS power	$\frac{K^{\text{SD}}}{K^{\text{SD}} + 1}$	$\frac{K^{\text{SR}}}{K^{\text{SR}} + 1}$	$\frac{K^{\text{RD}}}{K^{\text{RD}} + 1}$
NLoS power	$\frac{1}{(K^{\text{SD}} + 1)}$	$\frac{1}{(K^{\text{SR}} + 1)}$	$\frac{1}{(K^{\text{RD}} + 1)}$
Nor. Max. Dopp.	f_d^{SD}	f_d^{SR}	f_d^{RD}
LoS AoA	$\phi_0^{\text{SD}} = \arctan \frac{y_S - y_D}{x_S - x_D}$	$\phi_0^{\text{SR}} = \arctan \frac{y_S - y_R}{x_S - x_R}$	$\phi_0^{\text{RD}} = \arctan \frac{y_R - y_D}{x_R - x_D}$
RIS AoA		$\theta_R^{\text{AoA}} = \arccos \frac{z_S - z_R}{d^{\text{SR}}}$, $\varphi^{\text{AoA}} = \arctan \frac{y_S - y_R}{x_S - x_R}$	
RIS AoD			$\theta_R^{\text{AoD}} = \arccos \frac{z_D - z_R}{d^{\text{RD}}}$, $\varphi^{\text{AoD}} = \arctan \frac{y_D - y_R}{x_D - x_R}$
LoS offset	$\Delta f^{\text{SD,LoS}} = f_d^{\text{SD}} \cos(\phi_0^{\text{SD}})$	$\Delta f^{\text{SR,LoS}} = f_d^{\text{SR}} \cos(\phi_0^{\text{SR}})$	$\Delta f^{\text{RD,LoS}} = f_d^{\text{RD}} \cos(\phi_0^{\text{RD}})$

This is equivalent to the RIS optimization problem of MISO systems [4], which can be solved by the SDR technique. As discussed in Sec. I, this optimization method suffers from polynomial complexity as a function of N_T , N_R and M [3], which may become too complex to calculate for each sampling period in high-mobility scenarios.

In order to mitigate this problem, **the objective of the proposed AS is to align the RIS with a single RA index r^* , which leads to maximizing the channel's output power.** More explicitly, based on (5), the signal received at the r -th RA is given by $\mathbf{y}_n^r = (\mathbf{h}_n^{\text{SD}r} + \sum_{m=1}^M \alpha_n^m \mathbf{H}_n^{\text{SRD}r,m}) \mathbf{s}_n + \mathbf{v}_n^r$, where \mathbf{y}_n^r , $\mathbf{h}_n^{\text{SD}r}$ and \mathbf{v}_n^r refer to the r -th element in $\mathbf{y}_n \in \mathcal{C}^{N_R \times 1}$, $\mathbf{h}_n^{\text{SD}} \in \mathcal{C}^{N_R \times 1}$ and $\mathbf{v}_n \in \mathcal{C}^{N_R \times 1}$, respectively. As a result, maximizing the SNR for the chosen r^* -th RA leads to

$$\begin{aligned} & \max_{\{\alpha_n^m\}_{m=1}^M} \left| \mathbf{h}_n^{\text{SD}r^*} + \sum_{m=1}^M \alpha_n^m \mathbf{H}_n^{\text{SRD}r^*,m} \right|^2 \\ & = \max_{\{\alpha_n^m\}_{m=1}^M} \left| \mathbf{h}_n^{\text{SD}r^*} \right|^2 \left| \sum_{m=1}^M \beta_n^m \exp(jv_n^m) \right|^2, \end{aligned} \quad (7)$$

where we have $\beta_n^0 = 1$, $\{\beta_n^m = |\mathbf{H}_n^{\text{SRD}r^*,m}| / |\mathbf{h}_n^{\text{SD}r^*}|\}_{m=1}^M$, $v_n^0 = 0$ and $\{v_n^m = \angle \alpha_n^m + \angle \mathbf{H}_n^{\text{SRD}r^*,m} - \angle \mathbf{h}_n^{\text{SD}r^*}\}_{m=1}^M$. Bearing in mind that $\left| \sum_{m=0}^M \beta_n^m \exp(jv_n^m) \right|^2 = \sum_{m=0}^M |\beta_n^m|^2 + 2 \sum_{m=0}^M \sum_{m'=m+1}^M \beta_n^m \beta_n^{m'} \cos(v_n^m - v_n^{m'})$, (7) is maximized when $\{v_n^m = v_n^0\}_{\forall m}$, which leads to the RIS configuration of $\angle \alpha_n^m = \angle \mathbf{h}_n^{\text{SD}r^*} - \angle \mathbf{H}_n^{\text{SRD}r^*,m}$, or equivalently,

$$\alpha_n^m = \frac{\mathbf{h}_n^{\text{SD}r^*} \left(\mathbf{H}_n^{\text{SRD}r^*,m} \right)^*}{\left| \mathbf{h}_n^{\text{SD}r^*} \mathbf{H}_n^{\text{SRD}r^*,m} \right|}. \quad (8)$$

In order to determine r^* , we propose the following three AS algorithms. Firstly, the low-complexity *SD-max method* aligns all RIS elements to a single RA r^* based on the SD channel's output power in every time instant:

$$r^* = \arg \max_{\forall r} \left\| \mathbf{h}_n^{\text{SD}r} \right\|^2, \quad (9)$$

which does not require the CSI of the RIS-reflected links. Secondly, the *SRD-max method* aligns all RIS elements with a RA r^* based on the overall channel power in each sampling period:

$$\begin{aligned} r^* & = \arg \max_{\forall r} \sum_{r'=1}^{N_R} |\mathbf{h}_n^{\text{SD}r'} + \sum_{m=1}^M \alpha_n^m(r) \mathbf{H}_n^{\text{SRD}r',m}|^2 \\ & = \arg \max_{\forall r} \left\| \mathbf{h}_n^{\text{SD}} + \sum_{m=1}^M \alpha_n^m(r) \mathbf{H}_n^{\text{SRD},m} \right\|^2, \end{aligned} \quad (10)$$

where there are N_R candidates for the set $\alpha_n^m(r) = \frac{\mathbf{h}_n^{\text{SD}r} \left(\mathbf{H}_n^{\text{SRD}r,m} \right)^*}{\left| \mathbf{h}_n^{\text{SD}r} \mathbf{H}_n^{\text{SRD}r,m} \right|}$. Thirdly, for a full-search optimization (*FS-opt*)

method, each RIS element can be independently aligned to a RA as:

$$\begin{aligned} \{r_m^*\}_{m=1}^M & = \arg \max_{\forall \{r_m\}_{m=1}^M} \sum_{r'=1}^{N_R} |\mathbf{h}_n^{\text{SD}r'} + \sum_{m=1}^M \alpha_n^m(r_m) \mathbf{H}_n^{\text{SRD}r',m}|^2 \\ & = \arg \max_{\forall \{r_m\}_{m=1}^M} \left\| \mathbf{h}_n^{\text{SD}} + \sum_{m=1}^M \alpha_n^m(r_m) \mathbf{H}_n^{\text{SRD},m} \right\|^2, \end{aligned} \quad (11)$$

where there are a total of $(N_R)^M$ combinations for $\alpha_n^m(r_m) = \frac{\mathbf{h}_n^{\text{SD}r_m} \left(\mathbf{H}_n^{\text{SRD}r_m,m} \right)^*}{\left| \mathbf{h}_n^{\text{SD}r_m} \mathbf{H}_n^{\text{SRD}r_m,m} \right|}$ associated with $\{r_m = 1, \dots, N_R\}_{m=1}^M$. In order to alleviate the excessive full-search complexity, the random-search optimization (*RS-opt*) setup enumerates a subset combinations for $\alpha_n^m(r_m)$. In order to ensure a good performance for the RS-opt, the SRD-max method may be invoked first in order to initialize the random search. In summary, upon obtaining r^* by the SD-max of (9) or by the SRD-max of (10), the RIS configuration is completed by (8). For the FS/RS-opt of (11), the RIS configuration of (8) is

$$\text{modified as } \alpha_n^m = \frac{\mathbf{h}_n^{\text{SD}r^*} \left(\mathbf{H}_n^{\text{SRD}r^*,m} \right)^*}{\left| \mathbf{h}_n^{\text{SD}r^*} \mathbf{H}_n^{\text{SRD}r^*,m} \right|}.$$

The proposed RIS-AS algorithms are summarized in Table III, where \mathcal{N}_{RS} refers to the number of randomly generated combinations for RS-opt algorithm. The proposed AS algorithms belong to the family of RIS passive beamforming seen in Table I. In dynamic wireless communication, all RAs have the chance of being aligned by the RIS-AS, which leads to enhanced channel's output power over time, i.e. $E(\|\mathbf{h}_n\|^2)$ is maximized. Alternatively, the RA index for RIS alignment r^* may carry $\log_2 N_R$ IM bits facilitated by the RIS-SM concept of [40]–[44], which constitutes the benchmark in this paper.

C. Performance Analysis

The received signal model of (5) leads us to three key system performance metrics, namely the unconstrained capacity of continuous-input continuous-output memoryless channels (CCMC) that relies on idealistic Gaussian-input signals, the constrained capacity of discrete-input continuous-output memoryless channels (DCMC) that takes into account the realistic discrete-valued modulation schemes as well as the average BER.

Definition 1 (CCMC capacity): The CCMC capacity is given by maximizing the mutual information $I(s; \mathbf{y})$ between the channel's input and output signals over the distribution of $p(s)$ as $C^{\text{CCMC}}(SNR) = \max_{p(s)} I(s; \mathbf{y}) = \max_{p(s)} H(\mathbf{y}) - H(\mathbf{y}|s)$, where the entropies are maximized by the Gaussian input and output distributions, leading to $H(\mathbf{y}|s) = \log_2(\pi e N_0)$ and $H(\mathbf{y}) = \log_2[\pi e (\|\mathbf{h}_n\|^2 + N_0)]$. The ergodic CCMC capacity, which defines the maximum rate

TABLE III: The proposed RIS-AS algorithms.

SD-max	RS-opt
Input: \mathbf{h}_n^{SD} ; Output: $\{\alpha_n^m\}_{m=1}^M$; 1: $r^* = \arg \max_{\forall r} \ \mathbf{h}_n^{\text{SD}r}\ ^2$ 2: $\alpha_n^m = \mathbf{h}_n^{\text{SD}r^*} (\mathbf{H}_n^{\text{SRD}r^*,m})^* / \mathbf{h}_n^{\text{SD}r^*} \mathbf{H}_n^{\text{SRD}r^*,m} , \forall m$	Input: $\mathbf{h}_n^{\text{SD}}, \mathbf{H}_n^{\text{SRD}}, \mathcal{N}_{\text{RS}}$; Output: $\{\alpha_n^m\}_{m=1}^M$; 1: Invoke Steps 1-6 of SRD-max and obtain the initialized d_{max} and $r^* \cdot \{r_m^*\}_{m=1}^M$ are all initialized as $\{r_m^* = r^*\}_{m=1}^M$. 2: for $\iota = 1, 2, \dots, \mathcal{N}_{\text{RS}}$ 3: for $m = 1, 2, \dots, M$ 4: Randomly generate an integer r_m within $[1, N_R]$ 5: $\alpha_n^m(r_m) = \mathbf{h}_n^{\text{SD}r_m} (\mathbf{H}_n^{\text{SRD}r_m,m})^* / \mathbf{h}_n^{\text{SD}r_m} \mathbf{H}_n^{\text{SRD}r_m,m} $ 6: end for 7: $d_{\text{next}} = \ \mathbf{h}_n^{\text{SD}} + \sum_{m=1}^M \alpha_n^m(r_m) \mathbf{H}_n^{\text{SRD}-,m}\ ^2$ 8: if $d_{\text{next}} > d_{\text{max}}$: set $d_{\text{max}} = d_{\text{next}}$ and $r_m^* = r_m, \forall m$ 9: end for 10: $\alpha_n^m = \mathbf{h}_n^{\text{SD}r_m^*} (\mathbf{H}_n^{\text{SRD}r_m^*,m})^* / \mathbf{h}_n^{\text{SD}r_m^*} \mathbf{H}_n^{\text{SRD}r_m^*,m} , \forall m$
SRD-max	
Input: $\mathbf{h}_n^{\text{SD}}, \mathbf{H}_n^{\text{SRD}}$; Output: $\{\alpha_n^m\}_{m=1}^M$; 1: $d_{\text{max}} = 0$ 2: for $r = 1, 2, \dots, N_R$ 3: $\alpha_n^m(r) = \mathbf{h}_n^{\text{SD}r} (\mathbf{H}_n^{\text{SRD}r,m})^* / \mathbf{h}_n^{\text{SD}r} \mathbf{H}_n^{\text{SRD}r,m} , \forall m$ 4: $d_{\text{next}} = \ \mathbf{h}_n^{\text{SD}} + \sum_{m=1}^M \alpha_n^m(r) \mathbf{H}_n^{\text{SRD}-,m}\ ^2$ 5: if $d_{\text{next}} > d_{\text{max}}$: set $d_{\text{max}} = d_{\text{next}}$ and $r^* = r$ 6: end for 7: $\alpha_n^m = \mathbf{h}_n^{\text{SD}r^*} (\mathbf{H}_n^{\text{SRD}r^*,m})^* / \mathbf{h}_n^{\text{SD}r^*} \mathbf{H}_n^{\text{SRD}r^*,m} , \forall m$	

of $[H(\mathbf{y}) - H(\mathbf{y}|s)]$ averaged over all channel realizations of \mathbf{h}_n , may be formulated as:

$$C_{\text{RIS-AS}}^{\text{CCMC}}(\text{SNR}) = E \left[\log_2 \left(1 + \frac{\|\mathbf{h}_n\|^2}{N_0} \right) \right]. \quad (12)$$

The evaluation of (12) assumes full knowledge of $(\mathbf{h}_n = \mathbf{h}_n^{\text{SD}} + \sum_{m=1}^M \alpha_n^m \mathbf{H}_n^{\text{RD}-,m} \mathbf{h}_n^{\text{SRD}r_m})$ that incorporates the SD, SR and RD links, which are generated based on the Ricean distributions defined in Sec. III-A. The RIS is configured by the AS algorithms of Sec. III-B.

Definition 2 (DCMC capacity): In practice, the modulated PSK/QAM symbols constitute a non-Gaussian constellation for s_n of (5). In this scenario, the mutual information is maximized, when the modulated PSK/QAM symbols are equiprobable, i.e. we have $\{p(s^l) = \frac{1}{L}\}_{l=1}^L$, where $\{s^l\}_{l=1}^L$ refers to the L -PSK/QAM constellation points. As a result, the mutual information averaged over all channel realizations of \mathbf{h}_n becomes [62], [77] (13), where the conditional probability is formulated as $p(\mathbf{y}_n|s^l) = \frac{1}{\pi N_0} \exp(-\frac{\|\mathbf{y}_n - \mathbf{h}_n s^l\|^2}{N_0})$, while the throughput of RIS-AS is $R = \log_2 L$. Similarly, the DCMC capacity of RIS-SM is given by (14), where the conditional probability for RIS-SM is given by $p(\mathbf{y}_n|s^l, \mathbf{h}^{r^*}) = \frac{1}{\pi N_0} \exp(-\frac{\|\mathbf{y}_n - \mathbf{h}^{r^*} s^l\|^2}{N_0})$, while the throughput of RIS-SM is $R = \log_2 N_R L$. It can be readily seen that (13) and (14) are upper-bounded by $\log_2 L$ and $\log_2 N_R L$ bits, respectively, which verifies that RIS-SM is capable of achieving a higher bandwidth-efficiency than RIS-AS. However, in the next section, the two schemes will be compared under the same throughput, where L is increased for RIS-AS for a fair comparison. It is also worth noting that the DCMC capacity of (13) derived for RIS-AS and the DCMC capacity of (14) for RIS-SM are different from the capacity analysis of [33], which maximizes the overall achievable rate by modulating the RIS coefficients $\{\alpha_n^m\}_{m=1}^M$ as a set of M modulated PSK symbols. Both RIS-AS and RIS-SM are suitable for using large number of RIS elements for enhancing the SNR for a TA-RA pair, while the RIS-modulating scheme of [33] achieves the maximum throughput that is practical for a small number of RIS elements.

Definition 3 (Average BER): The average BER of RIS-AS is upper-bounded by:

$$P_e \leq \sum_{l=1}^L \sum_{l'=1}^L \frac{d_H(l, l')}{L \log_2 L} P(s^l \rightarrow s^{l'}), \quad (15)$$

where $d_H(l, l')$ refers to the Hamming distance between the bit-mappings, while $P(s^l \rightarrow s^{l'})$ is the pairwise error proba-

bility (PEP). The conditional PEP based on (5) is formulated as:

$$P(s^l \rightarrow s^{l'} | \mathbf{h}_n) = Q \left(\sqrt{\frac{\|\mathbf{h}_n(s^l - s^{l'})\|^2}{2N_0}} \right), \quad (16)$$

where the Q-function is given by $Q(x) = \frac{1}{\sqrt{2\pi}} \int_x^\infty \exp(-\frac{x^2}{2 \sin^2 \theta}) d\theta$. The PEP may be evaluated by averaging the conditional PEP over all channel realizations. To elaborate a little further, the moment generating function (MGF) of $\|\mathbf{h}_n(s^l - s^{l'})\|^2$ is given by [40], [44]:

$$\mathcal{M}(z) = \exp \left[\frac{z |s^l - s^{l'}|^2 \bar{\mathbf{h}}^H (\mathbf{I} - z |s^l - s^{l'}|^2 \mathbf{C}_h)^{-1} \bar{\mathbf{h}}}{\det(\mathbf{I} - z |s^l - s^{l'}|^2 \mathbf{C}_h)} \right], \quad (17)$$

where $\bar{\mathbf{h}}$ and \mathbf{C}_h are the mean vector and covariance matrix of \mathbf{h}_n . Let us recall that based on (5), we have $\mathbf{h}_n^r = \mathbf{h}_n^{\text{SD}r} + \sum_{m=1}^M \alpha_n^m \mathbf{H}_n^{\text{SRD}r,m}$ and $\mathbf{h}_n^{r^*} = \mathbf{h}_n^{\text{SD}r^*} \left(1 + \sum_{m=1}^M \frac{|\mathbf{H}_n^{\text{SRD}r^*,m}|}{|\mathbf{h}_n^{\text{SD}r^*}|} \right)$. According to the central limit theorem, the elements in \mathbf{h}_n converge to Gaussian distributions for large M . The mean and variance of the Gaussian-distributed variable \mathbf{h}_n^r are given by:

$$\begin{aligned} \mu_r &= \sqrt{\frac{K^{\text{SD}}}{1+K^{\text{SD}}}} + M \sqrt{\frac{K^{\text{SR}} K^{\text{RD}}}{(1+K^{\text{SR}})(1+K^{\text{RD}})}}, \\ \sigma_r^2 &= \frac{1}{1+K^{\text{SD}}} + \frac{M(1+K^{\text{SR}}+K^{\text{RD}})}{(1+K^{\text{SR}})(1+K^{\text{RD}})}, \end{aligned} \quad (18)$$

which are evaluated based on the component Gaussian distributions. Furthermore, the mean and variance of the Gaussian-distributed variable $\mathbf{h}_n^{r^*}$ are given by:

$$\begin{aligned} \mu_{r^*} &= \sqrt{\frac{K^{\text{SD}}}{1+K^{\text{SD}}}} + \frac{M\pi}{4} \sqrt{\frac{K^{\text{SR}} K^{\text{RD}}}{(1+K^{\text{SR}})(1+K^{\text{RD}})}} \mathcal{L}_{\frac{1}{2}}(-K^{\text{SR}}) \mathcal{L}_{\frac{1}{2}}(-K^{\text{RD}}), \\ \sigma_{r^*}^2 &= \frac{1}{1+K^{\text{SD}}} + M - \frac{M\pi^2}{16} \frac{\mathcal{L}_{\frac{1}{2}}^2(-K^{\text{SR}}) \mathcal{L}_{\frac{1}{2}}^2(-K^{\text{RD}})}{(1+K^{\text{SR}})(1+K^{\text{RD}})}, \end{aligned} \quad (19)$$

which are calculated based on the component Ricean-distributed amplitudes, where $\mathcal{L}_{\frac{1}{2}}(x)$ denotes the Laguerre polynomial. As a result, the conditional PEP of (16) is extended as:

$$P(s^l \rightarrow s^{l'} | r^*) = \frac{1}{\pi} \int_0^{\frac{\pi}{2}} \frac{\exp \left[-\frac{|s^l - s^{l'}|^2 \bar{\mathbf{h}}^H (\mathbf{I} + \frac{|s^l - s^{l'}|^2 \mathbf{C}_h}{4N_0 \sin^2 \theta})^{-1} \bar{\mathbf{h}}}{4N_0 \sin^2 \theta} \right]}{\det \left(\mathbf{I} + \frac{|s^l - s^{l'}|^2 \mathbf{C}_h}{4N_0 \sin^2 \theta} \right)} d\theta, \quad (20)$$

which is conditioned on the AS choice of r^* . For RIS-SM [40]–[44], the IM index r^* is part of the codeword, and the further extension of (20) depends on the choice of the RIS-SM's ML or greedy detection method. For RIS-AS, the choice of r^* depends on both the Doppler frequency and the AS methods of SD-max, SRD-max or FS/RS-opt. When the Doppler frequency is low, the receive powers of different RAs may change very slowly, which leads to the same r^* for a long period of time. However, as the mobility increases, r^* may vary more rapidly.

$$C_{\text{RIS-AS}}^{\text{DCMC}}(\text{SNR}) = \max_{\{p(s^l)\}_{l=1}^L} \sum_{l=1}^L \int p(\mathbf{y}_n | s^l) p(s^l) \log_2 \frac{p(\mathbf{y}_n | s^l)}{\sum_{l'=1}^L p(\mathbf{y}_n | s^{l'}) p(s^{l'})} d\mathbf{y} = \frac{1}{L} \sum_{l=1}^L E \left[\log_2 \frac{L p(\mathbf{y}_n | s^l)}{\sum_{l'=1}^L p(\mathbf{y}_n | s^{l'})} \right] \quad (13)$$

$$= R - \frac{1}{L} \sum_{l=1}^L E \left\{ \log_2 \left[\sum_{l'=1}^L \exp \left(-\frac{\|\mathbf{h}_n(s^l - s^{l'}) + \mathbf{v}_n\|^2 + \|\mathbf{v}_n\|^2}{N_0} \right) \right] \right\},$$

$$C_{\text{RIS-SM}}^{\text{DCMC}}(\text{SNR}) = \frac{1}{N_{R^*L}} \sum_{r^*=1}^{N_{R^*}} \sum_{l=1}^L E \left[\log_2 \frac{L p(\mathbf{y}_n | s^l, \mathbf{h}^{r^*})}{\sum_{r'^*=1}^{N_{R^*}} \sum_{l'=1}^L p(\mathbf{y}_n | s^{l'}, \mathbf{h}^{r'^*})} \right] \quad (14)$$

$$= R - \frac{1}{N_{R^*L}} \sum_{r^*=1}^{N_{R^*}} \sum_{l=1}^L E \left\{ \log_2 \left[\sum_{r'^*=1}^{N_{R^*}} \sum_{l'=1}^L \exp \left(-\frac{\|\mathbf{h}^{r^*} s^l - \mathbf{h}^{r'^*} s^{l'} + \mathbf{v}_n\|^2 + \|\mathbf{v}_n\|^2}{N_0} \right) \right] \right\},$$

TABLE IV: Summary of parameters for far-field propagation.

Initial coordinates	$(x_S, y_S, z_S) = (0, 0, 0)$, $(x_R, y_R, z_R) = (300, 4, 0)$, $(x_D, y_D, z_D) = (300, -2, 0)$
PLE	$\gamma^{\text{SR}} = \gamma^{\text{SD}} = 2.0$
Ricean K-factors	$K^{\text{SD}} = -6$ dB, $K^{\text{SR}} = 0$ dB, $K^{\text{DR}} = 0$ dB
Normalized maximum Doppler	$f_d^{\text{SD}} = f_d^{\text{RD}} = \frac{v f_c}{c f_s}$, $f_d^{\text{SR}} = 0$
Carrier frequency f_c	0.8 GHz (UHF-band), 1.5 GHz (L-band), 2.6 GHz (S-band), 4.7 GHz (C-band), 26 GHz (K-band), 38.5 GHz (Ka-band)
Antenna aperture	$A_e^S = 80$ cm ² , $A_e^D = 40$ cm ²
Bandwidth	100 kHz
Receiver noise power density	-174 dBm/Hz

D. Simulation Results

In this section, the simulation results of RIS assisted SIMO systems are presented in the context of far-field propagation conditions, as summarized in Table IV. For the CCMC capacity, DCMC capacity and BER results of Fig. 2 and Fig. 3, the PLE of the SD link is assumed to be $\gamma^{\text{SD}} = 4.08$ and the operating carrier frequency is assumed to be at 1.5 GHz (L-band). The effects of different locations of the car user, the different PLE γ^{SD} and the different carrier frequencies f_c are further investigated in Fig. 4.

Fig. 2 shows the CCMC and DCMC capacity results for RIS assisted SIMO scenarios. First of all, Figs. 2(a) and (b) confirm that in terms of CCMC capacity, the proposed RIS-AS is indeed capable of maximizing the SIMO channel power, where RIS-AS outperforms RIS using random phases without any optimization, followed by the case of only using the direct SD link without RIS. Secondly, Figs. 2(c) and (d) demonstrate that at a given system throughput, the proposed RIS-AS also outperforms the benchmark of RIS-SM. More explicitly, in contrast to the CCMC capacity of (12) relying on the idealistic and ‘Gaussianized’ channel’s input signals, the DCMC capacities of (13) and (14) rely on practical PSK/QAM signals that carry source bits. Therefore, the DCMC capacities of Figs. 2(c) and (d) converge to the same throughput R , but the proposed RIS-AS requires the lowest SNR for achieving the full throughput of $R = 2$ and $R = 4$ in Figs. 2(c) and (d), respectively. RIS-SM does not improve the propagation environment as much as the proposed RIS-AS, due to the fact that RIS-SM relies on the RIS alignment for conveying information bits instead of improving the SIMO channel power.

Fig. 3 portrays our BER performance results for RIS assisted SIMO. First of all, Figs. 3(a) and (b) once again confirm that the proposed RIS-AS achieves substantial performance improvements both over the RIS-SM benchmark and over the case of using the direct SD link without RIS. Secondly, when comparing different RIS-AS algorithms, Figs. 3(a) and (b) demonstrate that SRD-max achieves almost the same performance as RS-opt, where the RS-opt algorithms have exhaustively tested $\mathcal{N}_{RS} = 1000$ combinations

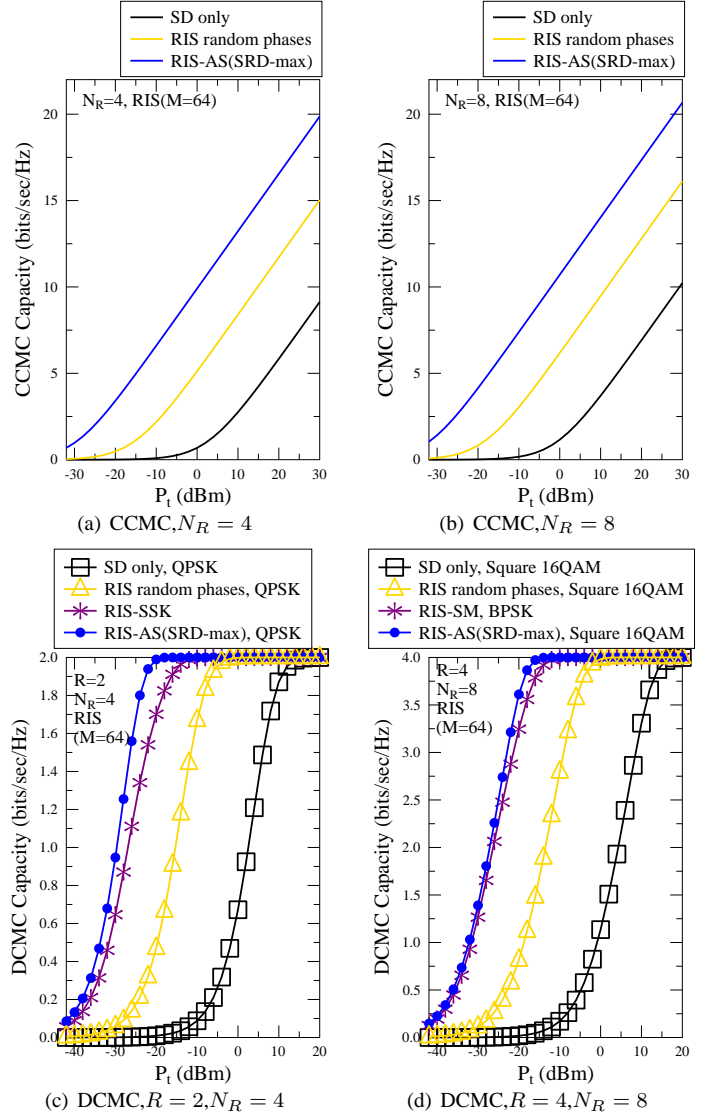


Fig. 2: CCMC capacity and DCMC capacity results for RIS assisted open-loop SIMO with CSI-R.

of independent RIS element alignments. This corroborates the effectiveness of the proposed SRD-max operating at linear complexity, where more exhaustive optimization search is no longer needed. Furthermore, Figs. 3(a) and (b) also demonstrate that SD-max which performs AS purely based on the direct SD link only suffers from a small performance loss compared to SRD-max and RS-opt, rendering SD-max an attractive choice for the scenario, when the CSI of the RIS-reflected links is not available at the instant of AS decision.

Fig. 4 summarizes the performance results for RIS assisted SIMO, where the power-efficiency is quantified in terms of the transmit power P_t (dBm) required for achieving the target BER of 10^{-4} . Fig. 4(a) investigates the effect of location,

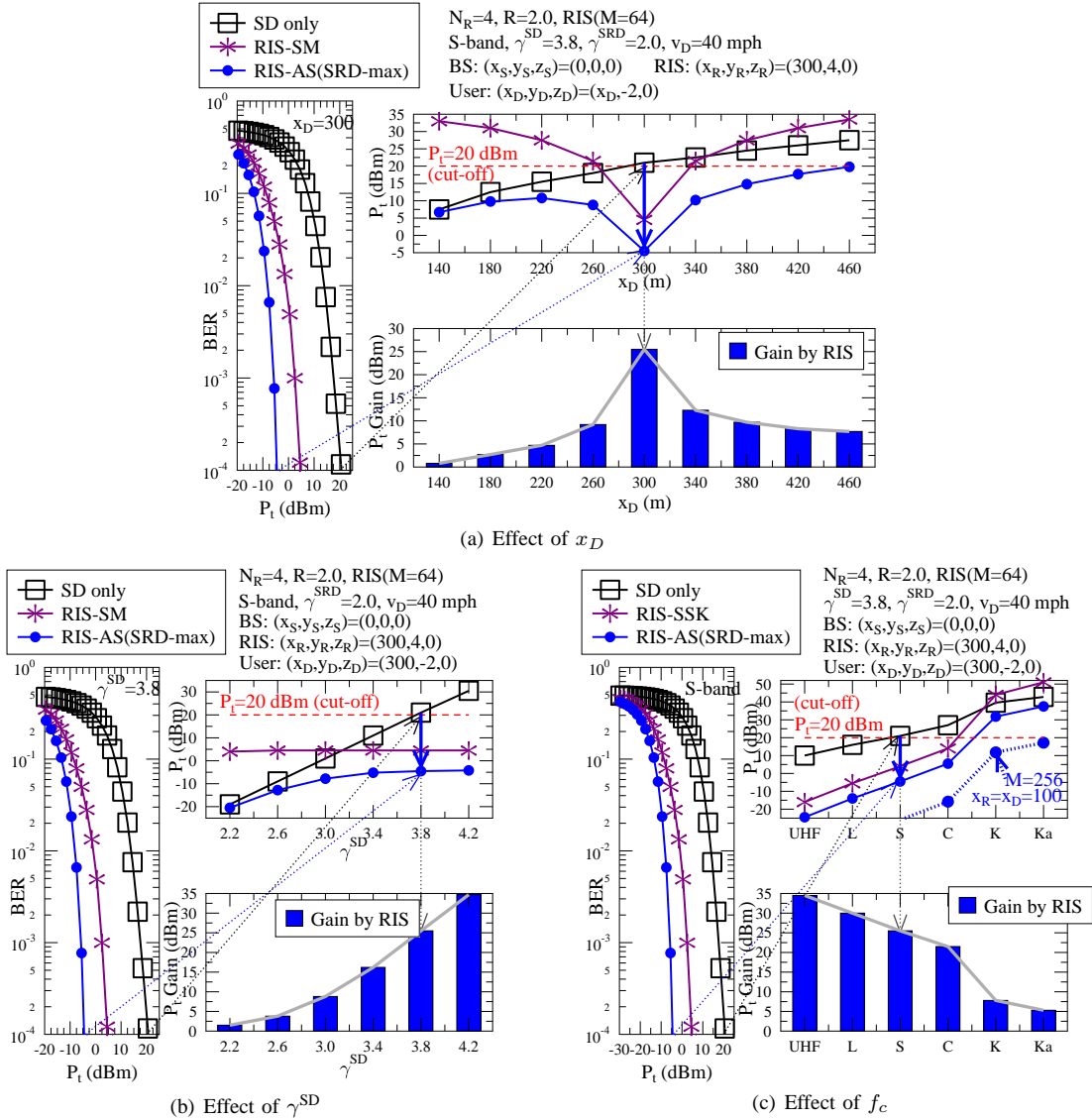


Fig. 4: Power-efficiency results for RIS assisted open-loop SIMO with CSI-R.

which demonstrates that the power-efficiency gain of using RIS-AS peaks when the car user is in the vicinity of the RIS. On one hand, when the car user moves closer to the BS, the direct link becomes strong enough even without RIS, as evidenced by Fig. 4(a). On the other hand, when the car user moves away, the direct link gradually loses coverage, which is indicated by the cut-off limit of $P_t = 20$ dBm in Fig. 4(a), but this is effectively mitigated by the proposed RIS-AS. Moreover, Fig. 4(a) also demonstrates that when the RIS-reflected links become weak, the RIS-SM benchmarker does not perform well. This is due to the fact that conveying extra information via RIS alignment becomes unreliable, unless the car user is close to the RIS location.

Furthermore, Fig. 4(b) investigates the effect of PLE, which may range from 2 to 6, depending on the blockage conditions [3]. It is demonstrated by Fig. 4(b) that the power-efficiency gain of the proposed RIS-AS manifests itself better when the PLE of the direct SD link increases, but the PLE of the SD link has almost no effect on the performance of RIS-SM, hence the SD link is often ignored in the RIS-SM literature [40]–[44].

Finally, Fig. 4(c) demonstrates the effect of the increasing carrier frequency, which induces a higher PL. As expected,

the power-efficiency gain achieved by the proposed RIS-AS decreases as f_c increases in Fig. 4(c), where the effective coverage can only be resumed in K-band and Ka-band by decreasing the distance between the BS and RIS and by increasing the RIS size.

IV. AS FOR RIS ASSISTED CLOSED-LOOP MISO BEAMFORMING WITH CSI-T

A. Received Signal Model

Firstly, the direct SD link is modelled as $\mathbf{h}_n^{SD} = \mathbf{h}_n^{SD,LoS} + \mathbf{h}_n^{SD,NLoS} \in \mathcal{C}^{1 \times N_T}$, where the LoS part is given by $\mathbf{h}_n^{SD,LoS} = \sqrt{\frac{K^{SD}}{1+K^{SD}}} \exp(j2\pi n \Delta f^{SD,LoS}) \mathbf{a}_{ULA}(\theta_S^{AoD})^H$, while the t -th element of the NLoS row vector $\mathbf{h}_n^{SD,NLoS}$ is associated with f_d^{SD} and $\mathbf{h}_n^{SD,NLoS,t} \sim \mathcal{CN}(0, \frac{1}{1+K^{SD}})$ for $(1 \leq t \leq N_T)$. Secondly, the SR link is given by $\mathbf{H}_n^{SR} = \mathbf{H}_n^{SR,LoS} + \mathbf{H}_n^{SR,NLoS} \in \mathcal{C}^{M \times N_T}$, where the LoS paths are modelled as $\mathbf{H}_n^{SR,LoS} = \sqrt{\frac{K^{SR}}{1+K^{SR}}} \exp(j2\pi n \Delta f^{SR,LoS}) \mathbf{a}_{UPA}(\theta_R^{AoA}, \varphi_R^{AoA}) \mathbf{a}_{ULA}(\theta_S^{AoD})^H$, while the NLoS element on the m -th row and t -th column of $\mathbf{H}_n^{SR,NLoS}$ is associated with f_d^{SR} and $\mathbf{H}_n^{SR,NLoS,m,t} \sim \mathcal{CN}(0, \frac{1}{1+K^{SR}})$ for $(1 \leq m \leq M)$

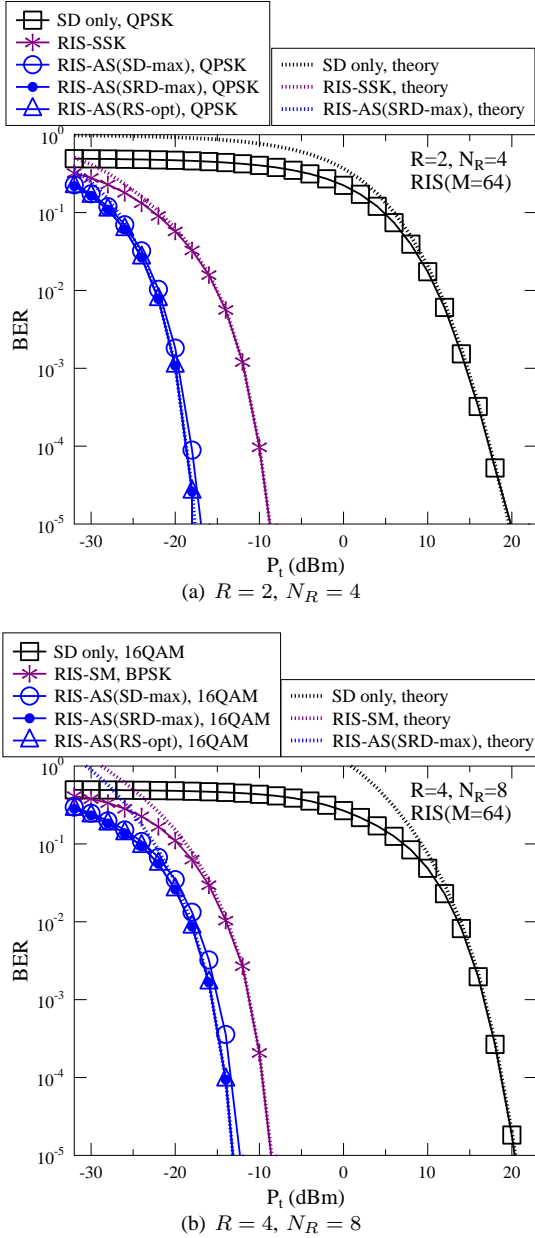


Fig. 3: BER results for RIS assisted open-loop SIMO with CSI-R.

and ($1 \leq t \leq N_T$). Thirdly, the RD link is $\mathbf{h}_n^{\text{RD}} = \mathbf{h}_n^{\text{RD,LoS}} + \mathbf{h}_n^{\text{RD,NLoS}} \in \mathcal{C}^{1 \times M}$, where $\mathbf{h}_n^{\text{RD,LoS}} = \sqrt{\frac{K^{\text{RD}}}{1+K^{\text{RD}}}} \exp(j2\pi n \Delta f^{\text{RD,LoS}}) \mathbf{a}_{\text{UPA}}(\theta_R^{\text{AoD}}, \varphi_R^{\text{AoD}})^H$ models the LoS, while the m -th NLoS element in $\mathbf{h}_n^{\text{RD,NLoS}}$ is associated with f_d^{RD} and $\mathbf{h}_n^{\text{RD,NLoS},m} \sim \mathcal{CN}(0, \frac{1}{1+K^{\text{RD}}})$ for ($1 \leq m \leq M$). As a result, the received signal is given by:

$$\begin{aligned} y_n &= \mathbf{h}_n \mathbf{w}_n s_n + v_n = (\mathbf{h}_n^{\text{SD}} + \sum_{m=1}^M \alpha_n^m \mathbf{h}_n^{\text{RD},m} \mathbf{H}_n^{\text{SR},m,-}) \mathbf{w}_n s_n + v_n \\ &= (\mathbf{h}_n^{\text{SD}} + \sum_{m=1}^M \alpha_n^m \mathbf{H}_n^{\text{SRD},m,-}) \mathbf{w}_n s_n + v_n, \end{aligned} \quad (21)$$

where $\mathbf{h}_n \in \mathcal{C}^{1 \times N_T}$ and $\mathbf{w}_n \in \mathcal{C}^{N_T \times 1}$ are the equivalent MISO channels and the BS beamforming vector, respectively. Moreover, $\mathbf{H}_n^{\text{SR},m,-}$ and $\mathbf{H}_n^{\text{SRD},m,-} = \mathbf{h}_n^{\text{RD},m} \mathbf{H}_n^{\text{SR},m,-}$ denote the m -th row in $\mathbf{H}_n^{\text{SR}} \in \mathcal{C}^{M \times N_T}$ and $\mathbf{H}_n^{\text{SRD}} \in \mathcal{C}^{M \times N_T}$, respectively, where $\mathbf{h}_n^{\text{RD},m}$ is the m -th element in \mathbf{h}_n^{RD} .

B. Problem Formulation and Antenna Selection Algorithms

The associated optimization problem is formulated as:

$$\max_{\{\alpha_n^m\}_{m=1}^M, \mathbf{w}_n} |\mathbf{h}_n \mathbf{w}_n|^2, \quad \text{s.t. } \{|\alpha_n^m| = 1\}_{m=1}^M \text{ and } E(\|\mathbf{w}_n\|^2) \leq 1. \quad (22)$$

The above non-convex problem may be solved by the low-complexity AO algorithm of [4]. On one hand, for a given beamforming vector \mathbf{w}_n , both the beamformed direct link $\mathbf{h}_n^{\text{SD}} \mathbf{w}_n$ and the beamformed RIS-reflected link $\mathbf{H}_n^{\text{SRD},m,-} \mathbf{w}_n$ become equivalent to SISO. Therefore, following (7), the optimum RIS configuration is given by $\angle \alpha_n^m = \angle \mathbf{h}_n^{\text{SD}} \mathbf{w}_n - \angle \mathbf{H}_n^{\text{SRD},m,-} \mathbf{w}_n$. On the other hand, for a given set of $\{\alpha_n^m\}_{m=1}^M$, the optimum beamforming vector is given by the maximum ratio transmission (MRT) of $\mathbf{w}_n = \frac{\mathbf{h}_n^H}{\|\mathbf{h}_n\|}$. Therefore, the AO algorithm [4] may iteratively optimize \mathbf{w}_n and $\{\alpha_n^m\}_{m=1}^M$ until the metric of (22) converges. However, the AO algorithm works better for static fading channels that remain unchanged over the period of signal transmission. In high-mobility scenarios, the AO algorithm has to be activated for each sampling period, with the number of iterations required for convergence varying with different system setups.

In order to mitigate this problem, the RIS-AS algorithms of Sec. III-B may be revised for beamforming based MISO systems, *where the objective of the proposed AS is to align the RIS with a single TA index t^* that leads to maximizing the channel's output power*. More explicitly, firstly, the SD-max method aligns all RIS elements with a single TA based on the direct SD link as $t^* = \arg \max_{t_t} \|\mathbf{h}_n^{\text{SD},t}\|^2$. Secondly, the SRD-max method aligns all RIS elements with a single TA based on the composite MISO channels as $t^* = \arg \max_{t_t} \|\mathbf{h}_n^{\text{SD}} + \sum_{m=1}^M \alpha_n^m(t) \mathbf{H}_n^{\text{SRD},m,-}\|^2$, where there are N_T candidates for the set $\alpha_n^m(t) = \frac{\mathbf{h}_n^{\text{SD},t} (\mathbf{H}_n^{\text{SRD},m,t})^*}{|\mathbf{h}_n^{\text{SD},t} \mathbf{H}_n^{\text{SRD},m,t}|}$ associated with ($t = 1, \dots, N_T$) and ($m = 1, \dots, M$). Thirdly, for the FS/RS-opt method, each RIS element can be independently configured to be aligned with a TA as $\{t_m^*\}_{m=1}^M = \arg \max_{\{t_m\}_{m=1}^M} \|\mathbf{h}_n^{\text{SD}} + \sum_{m=1}^M \alpha_n^m(t_m) \mathbf{H}_n^{\text{SRD},m,-}\|^2$, where there are $(N_T)^M$ combinations for $\alpha_n^m(t_m) = \frac{\mathbf{h}_n^{\text{SD},t_m} (\mathbf{H}_n^{\text{SRD},m,t_m})^*}{|\mathbf{h}_n^{\text{SD},t_m} \mathbf{H}_n^{\text{SRD},m,t_m}|}$ associated with $\{t_m = 1, \dots, N_T\}_{m=1}^M$. In summary, upon obtaining t^* by the SD-max or the SRD-max, the RIS is configured based on t^* as $\alpha_n^m = \frac{\mathbf{h}_n^{\text{SD},t^*} (\mathbf{H}_n^{\text{SRD},m,t^*})^*}{|\mathbf{h}_n^{\text{SD},t^*} \mathbf{H}_n^{\text{SRD},m,t^*}|}$. For the FS/RS-opt method, the RIS is configured based on $\{t_m^*\}_{m=1}^M$ as $\alpha_n^m = \frac{\mathbf{h}_n^{\text{SD},t_m^*} (\mathbf{H}_n^{\text{SRD},m,t_m^*})^*}{|\mathbf{h}_n^{\text{SD},t_m^*} \mathbf{H}_n^{\text{SRD},m,t_m^*}|}$. Finally, once the RIS is configured by the AS algorithms, the beamforming vector is given by the MRT of $\mathbf{w}_n = \frac{\mathbf{h}_n^H}{\|\mathbf{h}_n\|}$.

As a design alternative to the proposed RIS-AS, the RIS-SM is also configured by $\alpha_n^m = \frac{\mathbf{h}_n^{\text{SD},t^*} (\mathbf{H}_n^{\text{SRD},m,t^*})^*}{|\mathbf{h}_n^{\text{SD},t^*} \mathbf{H}_n^{\text{SRD},m,t^*}|}$ for ($m = 1, \dots, M$), where the TA index t^* conveys $\log_2 N_T$ IM bits [40]–[44].

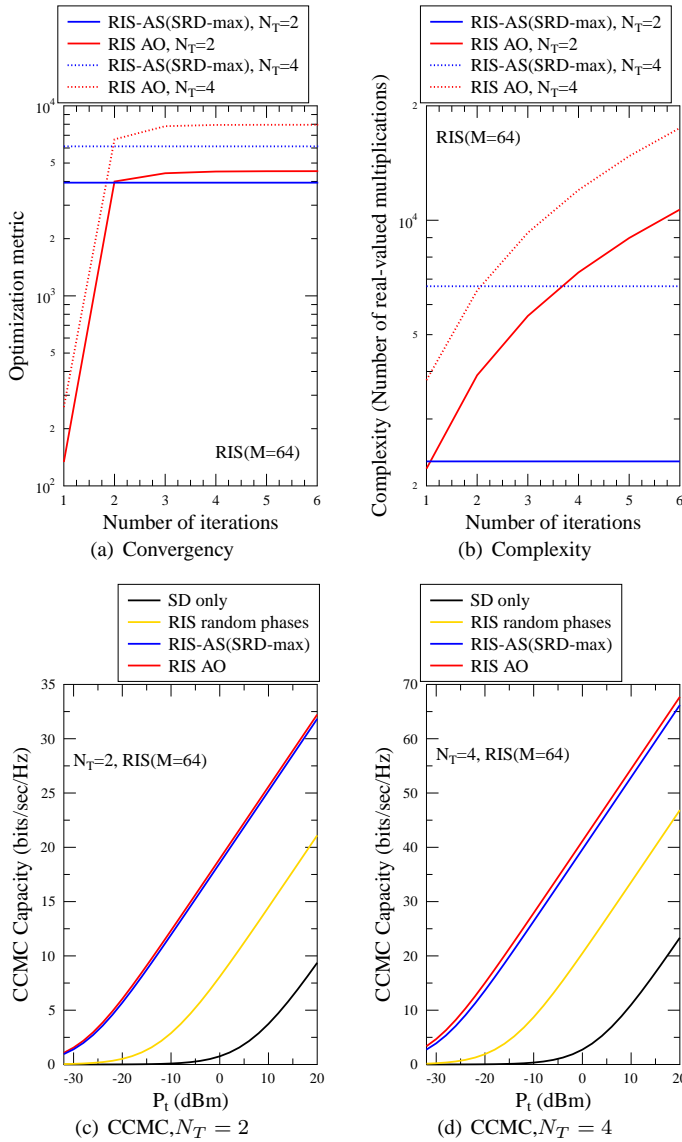


Fig. 5: Optimization convergence results for RIS assisted closed-loop MISO beamforming with CSI-T.

C. Performance Analysis

The received signal model of (21) is equivalent to a SISO system, where the fading element is given by $\tilde{h}_n = \mathbf{h}_n \mathbf{w}_n$. As a result, the CCMC capacity of (12), the DCMC capacity of (13) and the conditional PEP of (16) are now given by:

$$\begin{aligned}
 C_{\text{RIS-AS}}^{\text{CCMC}}(SNR) &= E \left[\log_2 \left(1 + \frac{|\tilde{h}_n|^2}{N_0} \right) \right], \\
 C_{\text{RIS-AS}}^{\text{DCMC}}(SNR) &= \log_2 L - \frac{1}{L} \sum_{l=1}^L E \left\{ \log_2 \left[\sum_{l'=1}^L \exp \left(-\frac{|\tilde{h}_n(s^l - s^{l'}) + v_n + |v_n|}{2N_0} \right) \right] \right\}, \\
 P(s^l \rightarrow s^{l'} | \tilde{h}_n) &= Q \left(\sqrt{\frac{|\tilde{h}_n(s^l - s^{l'})|^2}{2N_0}} \right).
 \end{aligned} \tag{23}$$

D. Simulation Results

In this section, we focus our attention on the optimization convergence, and a more detailed performance analysis will be provided for closed-loop MIMO beamforming in Sec. V. This is because the AO algorithm designed for RIS assisted closed-loop MIMO beamforming [7] has matrix inversions and decompositions whose complexity cannot be readily quantified. Hence the convergence complexity is analysed here for a MISO setup. The simulation parameters are the same as those presented in Sec. III-D.

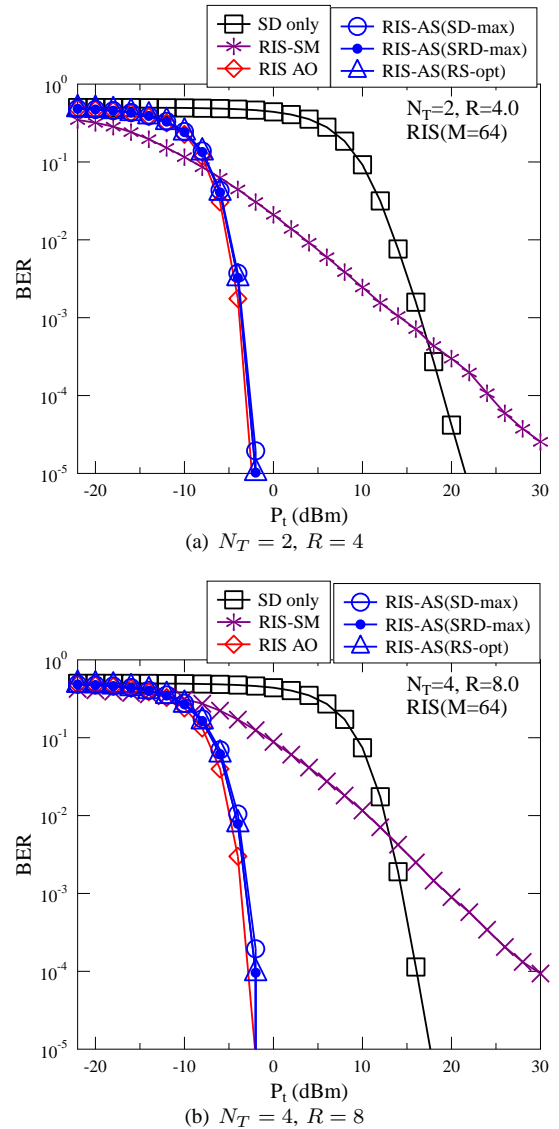


Fig. 6: BER results for RIS assisted closed-loop MISO beamforming with CSI-T.

Fig. 5(a) demonstrates that the AO algorithm [4] converges after five iterations, which achieves a higher optimization metric in terms of (22) than the proposed RIS-AS. However, Fig. 5(b) shows that the AO algorithm exhibits substantially higher complexity in terms of the number of real-valued multiplications than the proposed RIS-AS. Once again, we note that the proposed RIS-AS configures the RIS alone, i.e. without iterations with the transceiver optimization. Furthermore, Figs. 5(c) and (d) demonstrate that the optimization metric differences in Fig. 5(a) have very limited effect on performance, and that the proposed RIS-AS is capable of approaching the AO algorithm's CCMC capacity. Both the AO algorithm and the proposed RIS-AS achieve substantial performance advantages over the case of RIS using random phases and the case of using a direct SD link without RIS assistance, as demonstrated by Figs. 5(c) and (d).

Fig. 6 portrays our BER results for RIS assisted MISO beamforming, which confirms that both the SRD-opt and RS-opt methods of RIS-AS are capable of approaching the AO algorithm's performance. Moreover, the SD-max method is also capable of achieving substantial performance gain over

the case of using direct SD link without RIS, as evidenced by Fig. 6. Finally, Fig. 6 demonstrates that the RIS-SM benchmark does not perform well, when it is compared to the RIS-AS associated with the same throughput.

V. AS FOR RIS ASSISTED CLOSED-LOOP MIMO BEAMFORMING WITH CSI-T

A. Received Signal Model

The received signals of the RIS assisted MIMO beamforming are formulated as:

$$\begin{aligned} \mathbf{y}_n &= \mathbf{H}_n \mathbf{W}_n \mathbf{s}_n + \mathbf{v}_n \\ &= (\mathbf{H}_n^{\text{SD}} + \sum_{m=1}^M \alpha_n^m \mathbf{H}_n^{\text{RD},-m} \mathbf{H}_n^{\text{SR},m,-}) \mathbf{W}_n \mathbf{s}_n + \mathbf{v}_n, \end{aligned} \quad (24)$$

where we have $\mathbf{y}_n \in \mathcal{C}^{N_R \times 1}$, $\mathbf{H}_n \in \mathcal{C}^{N_R \times N_T}$, $\mathbf{W}_n \in \mathcal{C}^{N_T \times N_S}$, $\mathbf{s}_n \in \mathcal{C}^{N_S \times 1}$ and $\mathbf{v}_n \in \mathcal{C}^{N_R \times 1}$. The SD link is modelled as $\mathbf{H}_n^{\text{SD}} = \mathbf{H}_n^{\text{SD,LoS}} + \mathbf{H}_n^{\text{SD,NLoS}} \in \mathcal{C}^{N_R \times N_T}$, where the LoS part is given by $\mathbf{H}_n^{\text{SD,LoS}} = \sqrt{\frac{K^{\text{SD}}}{1+K^{\text{SD}}}} \exp(j2\pi n \Delta f^{\text{SD,LoS}}) \mathbf{a}_{\text{ULA}}(\theta_D^{\text{AoA}}) \mathbf{a}_{\text{ULA}}(\theta_S^{\text{AoD}})^H$, while the NLoS element on the r -th row and t -th column of $\mathbf{H}_n^{\text{SD,NLoS}}$ is associated with f_d^{SD} and $\mathbf{H}_n^{\text{SD,NLoS},r,t} \sim \mathcal{CN}(0, \frac{1}{1+K^{\text{SD}}})$ for $(1 \leq r \leq N_R)$ and $(1 \leq t \leq N_T)$. The SR link is generated in the same way as in the case of the RIS assisted MISO scheme of Sec. IV-A, while the RD link is generated in the same way as in the case of the RIS assisted SIMO arrangement of Sec. III-A.

B. Problem Formulation and Antenna Selection Algorithms

The corresponding optimization problem is formulated as:

$$\max_{\{\alpha_n^m\}_{m=1}^M, \mathbf{W}_n} \|\mathbf{H}_n \mathbf{W}_n\|^2, \quad \text{s.t. } \{|\alpha_n^m| = 1\}_{m=1}^M \text{ and } \|\mathbf{W}_n\|^2 \leq \text{same} \quad (25)$$

The AO algorithm is conceived for the above non-convex problem in [7]. When the RIS phases $\{\alpha_n^m\}_{m=1}^M$ are fixed, the optimal beamforming matrix \mathbf{W}_n is given by applying the SVD and waterfilling based on \mathbf{H}_n . On the other hand, when \mathbf{W}_n is decided, the RIS phases are solved one-by-one, assuming that all the others are fixed. However, this AO algorithm involves a total number of 1 SVD, M matrix inversions and $M+1$ EVDs for each iteration, which becomes unrealistic for frequent update in high-mobility scenarios.

In order to alleviate this problem, the AS algorithms of Secs. III-B and IV-B are revised for beamforming MIMO systems, *where the objective of the proposed AS is to align the RIS with a pair of TA-RA (t^*, r^*) that leads to maximizing the channel's output power.* Firstly, the SD-max method aligns all RIS elements to a TA-RA pair based on the SD channel power as $(t^*, r^*) = \arg \max_{\forall t, \forall r} \left\| \mathbf{H}_n^{\text{SD},r,t} \right\|^2$, and then the RIS is configured by $\alpha_n^m = \frac{\mathbf{H}_n^{\text{SD},r^*,t^*} \left(\mathbf{H}_n^{\text{RD},r^*,m} \mathbf{H}_n^{\text{SR},m,t^*} \right)^*}{\left| \mathbf{H}_n^{\text{SD},r^*,t^*} \mathbf{H}_n^{\text{RD},r^*,m} \mathbf{H}_n^{\text{SR},m,t^*} \right|}$. Secondly, the SRD-max method aligns all RIS elements with a TA-RA pair based on the composite beamformed MIMO channels as $(t^*, r^*) = \arg \max_{\forall (t,r)} \left\| \left(\mathbf{H}_n^{\text{SD}} + \sum_{m=1}^M \alpha_n^m(t,r) \mathbf{H}_n^{\text{RD},-m} \mathbf{H}_n^{\text{SR},m,-} \right) \mathbf{W}_n(t,r) \right\|^2$. There are $N_T N_R$ candidates for the TA-RA pair (t,r) , where the candidates $\{\mathbf{W}_n(t,r)\}_{\forall (t,r)}$ are configured by applying SVD and waterfilling to the RIS-assisted MIMO channels

configured by the set $\alpha_n^m(t,r) = \frac{\mathbf{H}_n^{\text{SD},r,t} \left(\mathbf{H}_n^{\text{RD},r,m} \mathbf{H}_n^{\text{SR},m,t} \right)^*}{\left| \mathbf{H}_n^{\text{SD},r,t} \mathbf{H}_n^{\text{RD},r,m} \mathbf{H}_n^{\text{SR},m,t} \right|}$ associated with $(m = 1, \dots, M)$. The optimum RIS phases and beamforming matrix are given by $\{\alpha_n^m(t^*, r^*)\}_{m=1}^M$ and $\mathbf{W}_n(t^*, r^*)$, respectively. Thirdly, for the FS/RS-opt method, each RIS element can be independently aligned with a TA-RA pair as $\{t_m^*, r_m^*\}_{m=1}^M = \arg \max_{\forall (\{t_m, r_m\}_{m=1}^M)} \left\| \left(\mathbf{H}_n^{\text{SD}} + \sum_{m=1}^M \alpha_n^m(t_m, r_m) \mathbf{H}_n^{\text{RD},-m} \mathbf{H}_n^{\text{SR},m,-} \right) \mathbf{W}_n(\{t_m, r_m\}_{m=1}^M) \right\|^2$. There are $(N_T N_R)^M$ legitimate combinations for $\{t_m, r_m\}_{m=1}^M$, where the candidates $\mathbf{W}_n(\{t_m, r_m\}_{m=1}^M)$ are configured based on $\alpha_n^m(t_m, r_m) = \frac{\mathbf{H}_n^{\text{SD},r_m,t_m} \left(\mathbf{H}_n^{\text{RD},r_m,m} \mathbf{H}_n^{\text{SR},m,t_m} \right)^*}{\left| \mathbf{H}_n^{\text{SD},r_m,t_m} \mathbf{H}_n^{\text{RD},r_m,m} \mathbf{H}_n^{\text{SR},m,t_m} \right|}$. Upon obtaining $\{t_m^*, r_m^*\}_{m=1}^M$, the optimum RIS phases and beamforming matrix are given by $\{\alpha_n^m(t_m^*, r_m^*)\}_{m=1}^M$ and $\mathbf{W}_n(\{t_m^*, r_m^*\}_{m=1}^M)$.

C. Performance Analysis

Upon applying SVD and transmit/receive beamforming, the received signal of (24) is decoupled into N_S SISO transmitted streams. As a result, the CCMC capacity, DCMC capacity and conditional PEP can also be evaluated by (23), where \tilde{h}_n is replaced by the real-valued power coefficient obtained by waterfilling.

D. Simulation Results

The CCMC capacity, DCMC capacity and the BER results of our RIS assisted MIMO beamforming are portrayed by Figs. 7 and 8, where the simulation parameters are the same as those presented in Sec. III-D. It is demonstrated by Figs. 7 and 8 that the RS-opt method of the proposed RIS-AS is capable of approaching the performance of the AO algorithm. Once again, the low-complexity RIS-AS only has to check on the channel's output power, while the classic AO algorithm of [7] involves the SVD/EVD and matrix inversions for each iteration. Furthermore, Fig. 8 demonstrates that the SRD-max method imposes a performance loss compared to the RS-opt, and the performance of the SD-max deteriorates even further. This is due to the specific nature of the SVD-based beamforming method that performs better when the singular values are maximized and balanced. This can be more readily achieved by the maximum degree of freedom provided by aligning different RIS elements to different TA-RA pairs.

VI. AS FOR RIS ASSISTED GENERIC OPEN-LOOP MIMO WITH CSI-R

A. Received Signal Model

The received signals of the RIS assisted generic MIMO system are modelled as:

$$\mathbf{Y}_n = \mathbf{H}_n \mathbf{S}_n + \mathbf{V}_n = (\mathbf{H}_n^{\text{SD}} + \sum_{m=1}^M \alpha_n^m \mathbf{H}_n^{\text{RD},-m} \mathbf{H}_n^{\text{SR},m,-}) \mathbf{S}_n + \mathbf{V}_n, \quad (26)$$

where in order to enable space-time signal transmission over T time slots, we have $\mathbf{Y}_n \in \mathcal{C}^{N_R \times T}$, $\mathbf{S}_n \in \mathcal{C}^{N_T \times T}$ and $\mathbf{V}_n \in \mathcal{C}^{N_R \times T}$. As a result, the received signal model of (26) is capable of supporting any MIMO signal transmission including V-BLAST, STBC, SM, STSK, GSM and GSTSK,

DRAFT

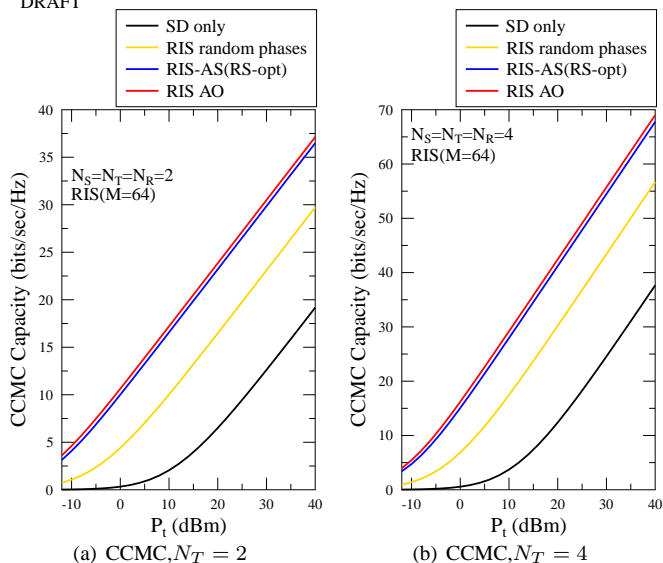


Fig. 7: CCMC and DCMC capacity results for RIS assisted closed-loop MIMO beamforming with CSI-T.

which may all be expressed in the dispersion matrix (DM) form [62] as $\mathbf{S} = \sum_{q=1}^Q \mathbf{A}_q s_q$, where $\{\mathbf{A}_q \in \mathcal{C}^{N_T \times T}\}_{q=1}^Q$ and $\{s_q\}_{q=1}^Q$ are DMs and modulated symbols, respectively. Firstly, for V-BLAST, we have ($Q = N_T$) and ($T = 1$), and the DMs are in the form of $\mathbf{A}_q = [0, \dots, 0, 1, 0, \dots, 0]^T$, where the position of the non-zero element is indicated by q . V-BLAST has the full-multiplexing MIMO throughput of ($R = N_T \log_2 L$). Secondly, the DMs for STBCs are designed for achieving both orthogonality and diversity gain, where the throughput is ($R = \frac{Q \log_2 L}{T}$). Thirdly, SM shares the same set of DMs with V-BLAST, but only one out of N_T DM is activated for the single-RF transmission as $\mathbf{S} = \mathbf{A}_q s^l$, where both the DM activation index q and the modulation index l convey information, leading to the throughput of ($R = \log_2 N_T + \log_2 L$). Thirdly, STSK also has the form of $\mathbf{S} = \mathbf{A}_q s^l$, where the DM design follows the STBC philosophy of maximizing the diversity gain, and the throughput is ($R = \frac{\log_2 Q + \log_2 L}{T}$). In the absence of multiplexing, both SM and STSK are free from inter-channel interference (ICI), which facilitates a single-antenna-based low-complexity signal detection at the receiver. In order to further improve their

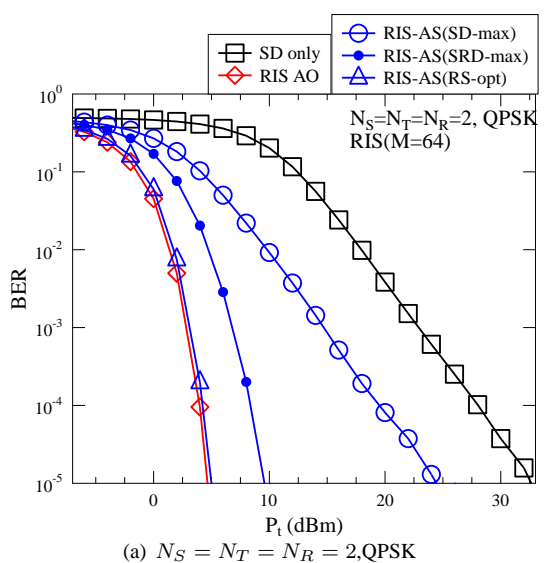


Fig. 8: BER results for RIS assisted closed-loop MIMO beamforming with CSI-T.

throughputs, GSM and GSTSK opt for activating more than one DMs, which however imposes a certain amount of ICI.

B. Problem Formulation and Antenna Selection Algorithms

The optimization problem is formulated as:

$$\begin{aligned} & \max_{\{\alpha_n^m\}_{m=1}^M} \|\mathbf{H}_n\|^2 \\ & = \max_{\{\alpha_n^m\}_{m=1}^M} \left\| \mathbf{H}_n^{\text{SD}} + \sum_{m=1}^M \alpha_n^m \mathbf{H}_n^{\text{RD},-m} \mathbf{H}_n^{\text{SR},m,-} \right\|^2, \quad (27) \\ & \text{s.t. } \{|\alpha_n^m| = 1\}_{m=1}^M. \end{aligned}$$

The AS algorithms of Secs. III-B, IV-B and V-B may be revised as low-complexity sub-optimal solutions of the above non-convex problem, *where the objective of the proposed AS is to align the RIS with a pair of TA-RA (t^*, r^*) that leads to maximizing the channel's output power*. More explicitly, firstly, the SD-max method aligns all RIS elements with a TA-RA pair as $(t^*, r^*) = \arg \max_{t \forall r} \|\mathbf{H}_n^{\text{SD},r,t}\|^2$. Secondly, the SRD-max method is revised to $(t^*, r^*) = \arg \max_{t \forall r} \left\| \mathbf{H}_n^{\text{SD}} + \sum_{m=1}^M \alpha_n^m(t, r) \mathbf{H}_n^{\text{RD},-m} \mathbf{H}_n^{\text{SR},m,-} \right\|^2$, where there are a total $N_T N_R$ candidates for $\alpha_n^m(t, r) = \frac{\mathbf{H}_n^{\text{SD},r,t} (\mathbf{H}_n^{\text{RD},r,m} \mathbf{H}_n^{\text{SR},m,t})^*}{|\mathbf{H}_n^{\text{SD},r,t} \mathbf{H}_n^{\text{RD},r,m} \mathbf{H}_n^{\text{SR},m,t}|}$. Finally, the FS/RS-opt method is

revised to $\{t_m^*, r_m^*\}_{m=1}^M = \arg \max_{\{t_m, r_m\}_{m=1}^M} \|(\mathbf{H}_n^{\text{SD}} + \sum_{m=1}^M \alpha_n^m(t_m, r_m) \mathbf{H}_n^{\text{RD}, -m} \mathbf{H}_n^{\text{SR}, m}) \mathbf{W}_n(\{t_m, r_m\}_{m=1}^M)\|^2$, where there are a total $(N_T N_R)^M$ combinations for $\alpha_n^m(t_m, r_m) = \frac{\mathbf{H}_n^{\text{SD}, r_m, t_m} (\mathbf{H}_n^{\text{RD}, r_m, m} \mathbf{H}_n^{\text{SR}, m, t_m})^*}{|\mathbf{H}_n^{\text{SD}, r_m, t_m} \mathbf{H}_n^{\text{RD}, r_m, m} \mathbf{H}_n^{\text{SR}, m, t_m}|}$. Upon obtaining (t^*, r^*) by the SD-max or the SRD-max, the RIS is configured by $\alpha_n^m = \frac{\mathbf{H}_n^{\text{SD}, r^*, t^*} (\mathbf{H}_n^{\text{RD}, r^*, m} \mathbf{H}_n^{\text{SR}, m, t^*})^*}{|\mathbf{H}_n^{\text{SD}, r^*, t^*} \mathbf{H}_n^{\text{RD}, r^*, m} \mathbf{H}_n^{\text{SR}, m, t^*}|}$. For the FS/RS-opt method, the RIS is configured based on $\{t_m^*, r_m^*\}_{m=1}^M$ as $\alpha_n^m = \frac{\mathbf{H}_n^{\text{SD}, r_m^*, t_m^*} (\mathbf{H}_n^{\text{RD}, r_m^*, m} \mathbf{H}_n^{\text{SR}, m, t_m^*})^*}{|\mathbf{H}_n^{\text{SD}, r_m^*, t_m^*} \mathbf{H}_n^{\text{RD}, r_m^*, m} \mathbf{H}_n^{\text{SR}, m, t_m^*}|}$.

C. Performance Analysis

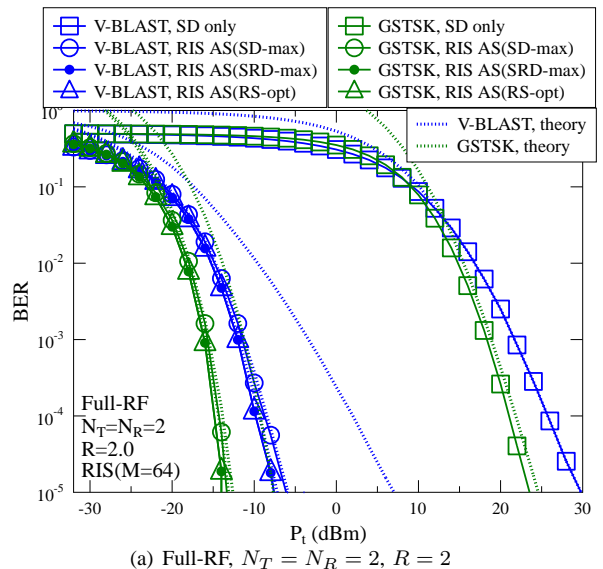
The performance analysis of RIS-assisted generic MIMO follows the methodologies of Secs. III-C, IV-C and V-C. The interested readers might like to refer to [62], [75]–[77] for the detailed performance analysis for using different MIMO codewords.

D. Simulation Results

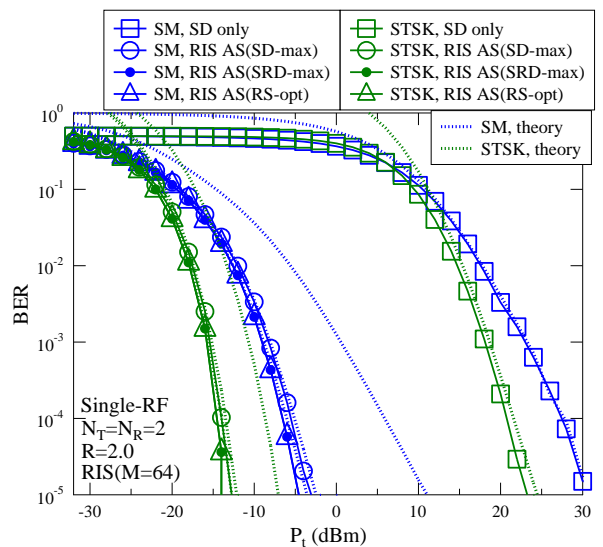
In this section, the RIS is harnessed for supporting full-/single-RF MIMO transmission. The simulation parameters are the same as those presented in Sec. III-D. As for full-RF MIMOs, both the multiplexing-oriented V-BLAST and diversity-oriented GSTSK are investigated. The GSTSK scheme of [63] activates N_T out of Q DMs, which results in the same level of ICI as V-BLAST. Moreover, the DMs in the GSTSK of [63] are designed to be sparse matrices which have non-zero elements at different positions, so that the superposition of $\sum_{q=1}^{N_T} \mathbf{A}_q s_q$ does not increase the peak-to-average power ratio (PAPR). On the other hand, for the single-RF MIMO, both the classic SM and STSK of [66] are supported by the RIS-assisted MIMO channels. More explicitly, the STSK of [66] activates one out of Q DMs, which are sparse matrices for ensuring single-RF, low-PAPR and ICI-free transmission. In summary, the diversity-oriented schemes of GSTSK and STSK are compared to their classic MIMO counterparts of V-BLAST and SM at the same transceiver complexity and the same throughput.

Fig. 9 portrays the BER results of our RIS-assisted MIMO schemes, which demonstrates that the proposed RIS-AS is capable of improving the performance of all the following MIMO schemes: V-BLAST, GSTSK, SM and STSK in both full-RF and single-RF modes. This verifies that the RIS-AS advocated improves the MIMO channels and are agnostic to the specific choice of the MIMO transceiver. Furthermore, Fig. 9 also demonstrates that the diversity-oriented GSTSK and STSK schemes are capable of achieving their intended diversity gains over V-BLAST and SM, respectively, in addition to their RIS gain.

Fig. 10 portrays our power-efficiency results for RIS assisted MIMO schemes, which once again confirms that the RIS achieves the maximum gain, when the car user is in the vicinity of the RIS location. Furthermore, it is evidenced by Fig. 10 that the diversity gains of GSTSK and STSK further improve the



(a) Full-RF, $N_T = N_R = 2$, $R = 2$



(b) Single-RF, $N_T = N_R = 2$, $R = 2$

Fig. 9: BER results for RIS assisted open-loop MIMO with CSI-R.

RIS-assisted MIMO transmission, where the car user satisfies the signal coverage threshold of $P_t = 20$ dBm over a wider range of distances from the BS.

VII. IMPACT OF RIS CHANNEL ESTIMATION

As for the RIS channel estimation methods, the ON/OFF based schemes [8], [71] estimate the CSI of the direct link first by switching off the RIS. Following this, the RIS-reflected links are successively estimated by activating a single RIS element in a time slot, where the estimated direct link is subtracted from the subsequent estimations. As a further improvement, the discrete Fourier transform (DFT) based methods of [9], [72], [73] activate all of the RIS elements based on the classic DFT matrix, so that the direct link and all reflected links become orthogonal. The pilot overhead can be reduced by grouping together a set of adjacent RIS elements [8] and upon configuring the RIS based on the statistical knowledge of the CSI [39], by compressive sensing [87], deep learning [88], codebook-based training [89] and matrix factorization [90], [91]. For high-mobility scenarios,

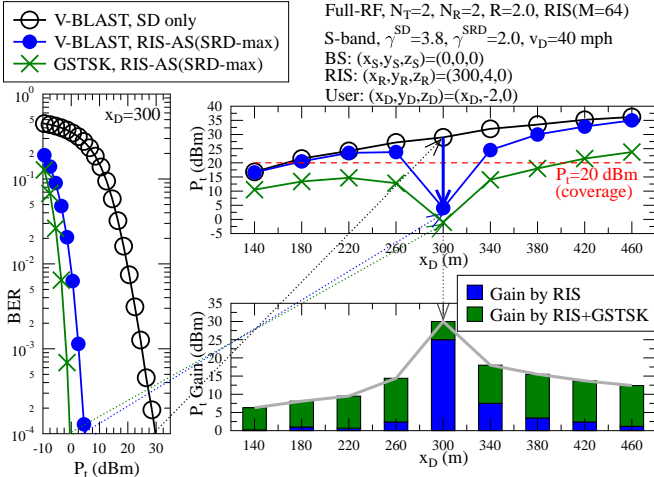
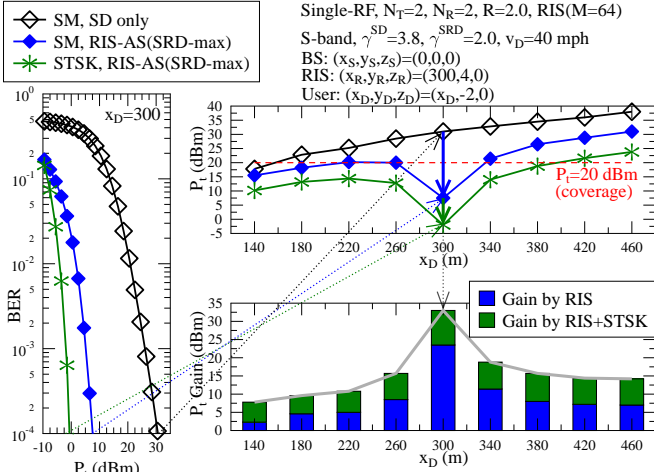
(a) Full-RF, $N_T = N_R = 2$, $R = 2$ (b) Single-RF, $N_T = N_R = 2$, $R = 2$

Fig. 10: Power-efficiency results for RIS assisted open-loop MIMO with CSI-R.

the RIS channel estimation that takes into account the Doppler frequency has been facilitated in both time-frequency domain and delay-Doppler domain in [55], [92], [93].

The impact of imperfect CSI is portrayed in Fig. 11 for open-loop SIMO/MIMO and closed-loop MISO¹ based on the Cramer-Rao bound in [92]. For SIMO/MIMO without beamforming, Figs. 11(a) and (b) demonstrate that the imperfect CSI-R degrades the performance of the proposed RIS-AS, because the inaccurate CSI is used for RIS configuration. Nonetheless, the proposed RIS-AS still substantially outperforms RIS-SM. In fact, RIS-SM requires CSI-T in order to configure RIS based on both IM bits and CSI, where the imperfect CSI feedback leads to error floors in Fig. 11(b). For closed-loop MISO, Figs. 11(c) and (d) evidence that the imperfect CSI feedback imposes more severe performance degradation on the AO algorithms than the proposed RIS-AS, owing to the fact that the RIS-AO's iterations lead to accumulated deviations in the presence of CSI errors.

¹We note that imperfect CSI would impose interference to the data streams in closed-loop MIMO, which requires further equalization at the receiver. In order to avoid digressing from the main focus, closed-loop MIMO is not shown in Fig. 11.

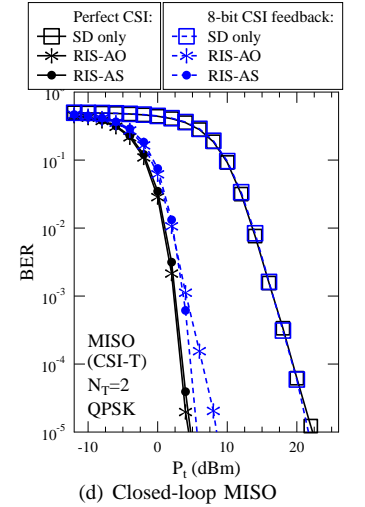
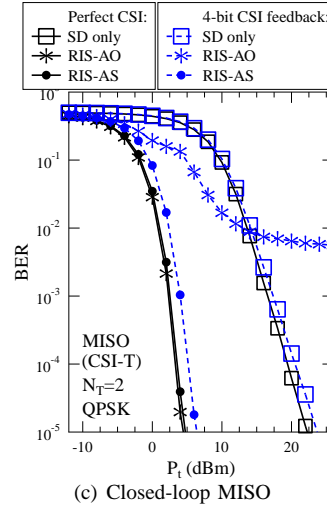
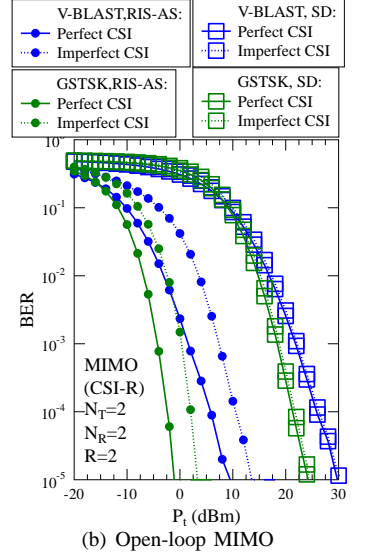
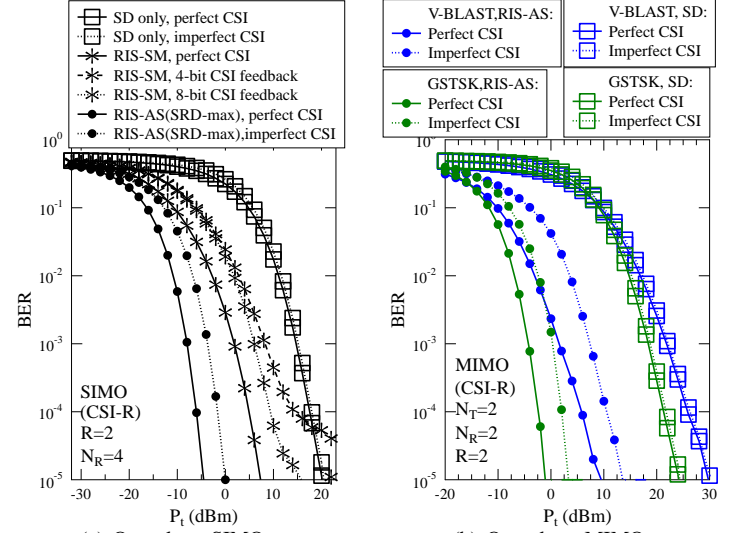


Fig. 11: BER results for RIS assisted SIMO/MISO/MIMO with imperfect CSI.

VIII. CONCLUSIONS

New RIS-AS algorithms were proposed in order to facilitate low-complexity independent RIS configuration. In response to the key questions posed in Sec. I, firstly, the RIS beamforming gain achieved by RIS-AS is shown to be more beneficial than the RIS reflection-based modulation of RIS-SM. Secondly, the proposed RIS-AS algorithms are demonstrated to be capable of approaching the joint optimization performance of the classic AO algorithm at a substantially reduced complexity. Finally, the proposed RIS-AS improves the channel's output power and are agnostic to the specific choice of the MIMO transceiver. Our simulation results demonstrate that the proposed RIS-AS is capable of supporting any MIMO schemes, regardless of whether they have closed/open-loop, single-/full-RF and multiplexing-/diversity-oriented setups.

REFERENCES

- [1] S. Gong, X. Lu, D. T. Hoang, D. Niyato, L. Shu, D. I. Kim, and Y. Liang, "Towards smart wireless communications via intelligent reflecting surfaces: A contemporary survey," *IEEE Commun. Surveys Tut.*, vol. 22, no. 4, pp. 2283–2314, 2020.

- [2] M. D. Renzo, A. Zappone, M. Debbah, M. Alouini, C. Yuen, J. de Rosny, and S. Tretyakov, "Smart radio environments empowered by reconfigurable intelligent surfaces: How it works, state of research, and the road ahead," *IEEE J. Sel. Areas Commun.*, vol. 38, no. 11, pp. 2450–2525, 2020.
- [3] Q. Wu, S. Zhang, B. Zheng, S. You, and R. Zhang, "Intelligent reflecting surface-aided wireless communications: A tutorial," *IEEE Trans. Commun.*, vol. 69, no. 5, pp. 3313–3351, 2021.
- [4] Q. Wu and R. Zhang, "Intelligent reflecting surface enhanced wireless network via joint active and passive beamforming," *IEEE Trans. Wireless Commun.*, vol. 18, no. 11, pp. 5394–5409, 2019.
- [5] X. Yu, D. Xu, and R. Schober, "Optimal beamforming for MISO communications via intelligent reflecting surfaces," in *2020 IEEE 21st Int. Workshop Signal Process. Advances Wireless Commun. (SPAWC)*, 2020.
- [6] K. Feng, Q. Wang, X. Li, and C. Wen, "Deep reinforcement learning based intelligent reflecting surface optimization for MISO communication systems," *IEEE Wireless Commun. Lett.*, vol. 9, no. 5, pp. 745–749, 2020.
- [7] S. Zhang and R. Zhang, "Capacity characterization for intelligent reflecting surface aided MIMO communication," *IEEE J. Sel. Areas Commun.*, vol. 38, no. 8, pp. 1823–1838, 2020.
- [8] Y. Yang, B. Zheng, S. Zhang, and R. Zhang, "Intelligent reflecting surface meets OFDM: Protocol design and rate maximization," *IEEE Trans. Commun.*, vol. 68, no. 7, pp. 4522–4535, 2020.
- [9] B. Zheng and R. Zhang, "Intelligent reflecting surface-enhanced OFDM: Channel estimation and reflection optimization," *IEEE Wireless Commun. Lett.*, vol. 9, no. 4, pp. 518–522, 2020.
- [10] Q. Wu and R. Zhang, "Beamforming optimization for wireless network aided by intelligent reflecting surface with discrete phase shifts," *IEEE Trans. Commun.*, vol. 68, no. 3, pp. 1838–1851, 2020.
- [11] P. Xu, G. Chen, Z. Yang, and M. D. Renzo, "Reconfigurable intelligent surfaces-assisted communications with discrete phase shifts: How many quantization levels are required to achieve full diversity?," *IEEE Wireless Commun. Lett.*, vol. 10, no. 2, pp. 358–362, 2021.
- [12] Z. Xing, R. Wang, J. Wu, and E. Liu, "Achievable rate analysis and phase shift optimization on intelligent reflecting surface with hardware impairments," *accepted by IEEE Trans. Wireless Commun.*, 2021.
- [13] T. V. Chien, H. Q. Ngo, S. Chatzinotas, M. D. Renzo, and B. Ottersten, "Reconfigurable intelligent surface-assisted cell-free massive MIMO systems over spatially-correlated channels," *IEEE Trans. Wireless Commun.*, no. 7, pp. 5106–5128, 2022.
- [14] J. Ye, S. Guo, and M.-S. Alouini, "Joint reflecting and precoding designs for SER minimization in reconfigurable intelligent surfaces assisted MIMO systems," *IEEE Trans. Wireless Commun.*, vol. 19, no. 8, pp. 5561–5574, 2020.
- [15] C. Huang, A. Zappone, G. C. Alexandropoulos, M. Debbah, and C. Yuen, "Reconfigurable intelligent surfaces for energy efficiency in wireless communication," *IEEE Trans. Wireless Commun.*, vol. 18, no. 8, pp. 4157–4170, 2019.
- [16] C. Pan, H. Ren, K. Wang, W. Xu, M. ElKashlan, A. Nallanathan, and L. Hanzo, "Multicell MIMO communications relying on intelligent reflecting surfaces," *IEEE Trans. Wireless Commun.*, vol. 19, no. 8, pp. 5218–5233, 2020.
- [17] Y. Zhang, B. Di, H. Zhang, J. Lin, C. Xu, D. Zhang, Y. Li, and L. Song, "Beyond cell-free MIMO: Energy efficient reconfigurable intelligent surface aided cell-free MIMO communications," *IEEE Trans. Cognitive Commun. Network.*, vol. 7, no. 2, pp. 412–426, 2021.
- [18] G. Yang, X. Xu, Y. Liang, and M. D. Renzo, "Reconfigurable intelligent surface-assisted non-orthogonal multiple access," *IEEE Trans. Wireless Commun.*, vol. 20, no. 5, pp. 3137–3151, 2021.
- [19] T. Hou, Y. Liu, Z. Song, X. Sun, Y. Chen, and L. Hanzo, "Reconfigurable intelligent surface aided NOMA networks," *IEEE J. Sel. Areas Commun.*, vol. 38, no. 11, pp. 2575–2588, 2020.
- [20] T. Bai, C. Pan, Y. Deng, M. ElKashlan, A. Nallanathan, and L. Hanzo, "Latency minimization for intelligent reflecting surface aided mobile edge computing," *IEEE J. Sel. Areas Commun.*, vol. 38, no. 11, pp. 2666–2682, 2020.
- [21] X. Hu, C. Masouros, and K. K. Wong, "Reconfigurable intelligent surface aided mobile edge computing: From optimization-based to location-only learning-based solutions," *IEEE Trans. Commun.*, vol. 69, no. 6, pp. 3709–3725, 2021.
- [22] C. Pan, H. Ren, K. Wang, M. ElKashlan, A. Nallanathan, J. Wang, and L. Hanzo, "Intelligent reflecting surface aided MIMO broadcasting for simultaneous wireless information and power transfer," *IEEE J. Sel. Areas Commun.*, vol. 38, no. 8, pp. 1719–1734, 2020.
- [23] Q. Wu and R. Zhang, "Joint active and passive beamforming optimization for intelligent reflecting surface assisted SWIPT under QoS constraints," *IEEE J. Sel. Areas Commun.*, vol. 38, no. 8, pp. 1735–1748, 2020.
- [24] J. Chen, Y. Liang, Y. Pei, and H. Guo, "Intelligent reflecting surface: A programmable wireless environment for physical layer security," *IEEE Access*, vol. 7, pp. 82599–82612, 2019.
- [25] B. Feng, Y. Wu, M. Zheng, X.-G. Xia, Y. Wang, and C. Xiao, "Large intelligent surface aided physical layer security transmission," *IEEE Trans. Signal Process.*, vol. 68, pp. 5276–5291, 2020.
- [26] M. D. Renzo, M. Debbah, D. T. Phan-Huy, A. Zappone, M. S. Alouini, C. Yuen, V. Sciancalepore, G. C. Alexandropoulos, J. Hoydis, H. Gacanin, and J. D. Rosny, "Smart radio environments empowered by reconfigurable AI meta-surfaces: An idea whose time has come," *EURASIP J. Wireless Commun. Netw.*, 2019.
- [27] N. V. Huynh, D. T. Hoang, X. Lu, D. Niyato, P. Wang, and D. I. Kim, "Ambient backscatter communications: A contemporary survey," *IEEE Commun. Surveys Tuts.*, vol. 20, no. 4, pp. 2889–2922, 2018.
- [28] W. Tang, X. Li, J. Y. Dai, S. Jin, Y. Zeng, Q. Cheng, and T. J. Cui, "Wireless communications with programmable metasurface: Transceiver design and experimental results," *China Commun.*, vol. 16, no. 5, pp. 46–61, 2019.
- [29] W. Tang, M. Z. Chen, J. Y. Dai, Y. Zeng, X. Zhao, S. Jin, Q. Cheng, and T. J. Cui, "Wireless communications with programmable metasurface: New paradigms, opportunities, and challenges on transceiver design," *IEEE Wireless Commun.*, vol. 27, no. 2, pp. 180–187, 2020.
- [30] W. Tang, J. Y. Dai, M. Z. Chen, K.-K. Wong, X. Li, X. Zhao, S. Jin, Q. Cheng, and T. J. Cui, "MIMO transmission through reconfigurable intelligent surface: System design, analysis, and implementation," *IEEE J. Sel. Areas Commun.*, vol. 38, no. 11, pp. 2683–2699, 2020.
- [31] A. Khaleel and E. Basar, "Reconfigurable intelligent surface-empowered MIMO systems," *IEEE Systems J.*, pp. 1–9, 2020.
- [32] E. Basar, M. Di Renzo, J. De Rosny, M. Debbah, M. Alouini, and R. Zhang, "Wireless communications through reconfigurable intelligent surfaces," *IEEE Access*, vol. 7, pp. 116753–116773, 2019.
- [33] R. Karasik, O. Simeone, M. D. Renzo, and S. Shamai, "Adaptive coding and channel shaping through reconfigurable intelligent surfaces: An information-theoretic analysis," *IEEE Trans. Commun.*, vol. 69, no. 11, pp. 7320–7334, 2021.
- [34] Q. Li, M. Wen, S. Wang, G. C. Alexandropoulos, and Y.-C. Wu, "Space shift keying with reconfigurable intelligent surfaces: Phase configuration designs and performance analysis," *IEEE Open J. Commun. Society*, vol. 2, pp. 322–333, 2021.
- [35] S. Guo, S. Lv, H. Zhang, J. Ye, and P. Zhang, "Reflecting modulation," *IEEE J. Sel. Areas Commun.*, vol. 38, no. 11, pp. 2548–2561, 2020.
- [36] E. Basar, M. Wen, R. Mesleh, M. D. Renzo, Y. Xiao, and H. Haas, "Index modulation techniques for next-generation wireless networks," *IEEE Access*, vol. 5, pp. 16693–16746, 2017.
- [37] N. Ishikawa, S. Sugiura, and L. Hanzo, "50 years of permutation, spatial and index modulation: From classic rf to visible light communications and data storage," *IEEE Commun. Surveys Tut.*, vol. 20, no. 3, pp. 1905–1938, 2018.
- [38] W. Yan, X. Yuan, Z.-Q. He, and X. Kuai, "Passive beamforming and information transfer design for reconfigurable intelligent surfaces aided multiuser MIMO systems," *IEEE J. Sel. Areas Commun.*, vol. 38, no. 8, pp. 1793–1808, 2020.
- [39] S. Lin, B. Zheng, G. C. Alexandropoulos, M. Wen, M. D. Renzo, and F. Chen, "Reconfigurable intelligent surfaces with reflection pattern modulation: Beamforming design and performance analysis," *IEEE Trans. Wireless Commun.*, vol. 20, no. 2, pp. 741–754, 2021.
- [40] E. Basar, "Reconfigurable intelligent surface-based index modulation: A new beyond MIMO paradigm for 6G," *IEEE Trans. Commun.*, vol. 68, no. 5, pp. 3187–3196, 2020.
- [41] H. Albinsaid, K. Singh, A. Bansal, S. Biswas, C.-P. Li, and Z. J. Haas, "Multiple antenna selection and successive signal detection for SM-based IRS-aided communication," *IEEE Signal Process. Lett.*, vol. 28, pp. 813–817, 2021.
- [42] A. E. Cambilen, E. Basar, and S. S. Ikki, "Reconfigurable intelligent surface-assisted space shift keying," *IEEE Wireless Commun. Lett.*, vol. 9, no. 9, pp. 1495–1499, 2020.
- [43] J. Yuan, M. Wen, Q. Li, E. Basar, G. C. Alexandropoulos, and G. Chen, "Receive quadrature reflecting modulation for RIS-empowered wireless communications," *IEEE Trans. Veh. Technol.*, vol. 70, no. 5, pp. 5121–5125, 2021.
- [44] T. Ma, Y. Xiao, X. Lei, P. Yang, X. Lei, and O. A. Dobre, "Large intelligent surface assisted wireless communications with spatial modulation

- and antenna selection," *IEEE J. Sel. Areas Commun.*, vol. 38, no. 11, pp. 2562–2574, 2020.
- [45] R. Liu, M. Li, Q. Liu, and A. L. Swindlehurst, "Joint symbol-level precoding and reflecting designs for IRS-enhanced MU-MISO systems," *IEEE Trans. Wireless Commun.*, vol. 20, no. 2, pp. 798–811, 2021.
- [46] Z. Yang, M. Chen, W. Saad, W. Xu, M. Shikh-Bahaei, H. V. Poor, and S. Cui, "Energy-efficient wireless communications with distributed reconfigurable intelligent surfaces," *IEEE Trans. Wireless Commun.*, vol. 21, no. 1, pp. 665–679, 2022.
- [47] S. Jia, X. Yuan, and Y.-C. Liang, "Reconfigurable intelligent surfaces for energy efficiency in D2D communication network," *IEEE Wireless Commun. Lett.*, vol. 10, no. 3, pp. 683–687, 2021.
- [48] S. Jia, X. Yuan, and Y.-C. Liang, "What will 6G be?," *Nat. Electron.*, vol. 30, pp. 20–29, 2022.
- [49] W. Saad, M. Bennis, and M. Chen, "A vision of 6G wireless systems: Applications, trends, technologies, and open research problems," *IEEE Network*, vol. 34, no. 3, pp. 134–142, 2020.
- [50] C. Xu, N. Ishikawa, R. Rajashekar, S. Sugiura, R. G. Maunder, Z. Wang, L. Yang, and L. Hanzo, "Sixty years of coherent versus non-coherent tradeoffs and the road from 5G to wireless futures," *IEEE Access*, vol. 7, pp. 178246–178299, 2019.
- [51] J. Liu, Y. Shi, Z. Fadlullah, and N. Kato, "Space-air-ground integrated network: A survey," *IEEE Commun. Surveys Tuts.*, vol. 20, no. 4, pp. 2714–2741, 2018.
- [52] C. Xu, J. Zhang, T. Bai, P. Botsinis, R. G. Maunder, R. Zhang, and L. Hanzo, "Adaptive coherent/non-coherent single/multiple-antenna aided channel coded ground-to-air aeronautical communication," *IEEE Trans. Commun.*, vol. 67, no. 2, pp. 1099–1116, 2019.
- [53] C. Xu, T. Bai, J. Zhang, R. Rajashekar, R. G. Maunder, Z. Wang, and L. Hanzo, "Adaptive coherent/non-coherent spatial modulation aided unmanned aircraft systems," *IEEE Wireless Commun.*, vol. 26, no. 4, pp. 170–177, 2019.
- [54] X. Huang, J. Zhang, R. Liu, Y. Guo, and L. Hanzo, "Airplane-aided integrated networking for 6G wireless: Will it work?," *IEEE Veh. Technol. Mag.*, vol. 14, no. 3, pp. 84–91, 2019.
- [55] C. Xu, L. Xiang, J. An, C. Dong, S. Sugiura, R. G. Maunder, L. L. Yang, and L. Hanzo, "OTFS-aided RIS-assisted SAGIN systems outperform their OFDM counterparts in doubly-selective high-doppler scenarios," *IEEE Internet Things J.*, 2022.
- [56] M. Giordani, M. Polese, A. Roy, D. Castor, and M. Zorzi, "A tutorial on beam management for 3GPP NR at mmWave frequencies," *IEEE Commun. Surveys Tuts.*, vol. 21, no. 1, pp. 173–196, 2019.
- [57] X. Cao, B. Yang, C. Huang, C. Yuen, M. D. Renzo, Z. Han, D. Niyato, H. V. Poor, and L. Hanzo, "AI-assisted MAC for reconfigurable intelligent-surface-aided wireless networks: Challenges and opportunities," *IEEE Commun. Mag.*, vol. 59, no. 6, pp. 21–27, 2021.
- [58] O. Ozdogan, E. Bjornson, and E. G. Larsson, "Intelligent reflecting surfaces: Physics, propagation, and pathloss modeling," *IEEE Wireless Commun. Lett.*, vol. 9, no. 5, pp. 581–585, 2020.
- [59] W. Tang, M. Z. Chen, X. Chen, J. Y. Dai, Y. Han, M. D. Renzo, Y. Zeng, S. Jin, Q. Cheng, and T. J. Cui, "Wireless communications with reconfigurable intelligent surface: Path loss modeling and experimental measurement," *IEEE Trans. Wireless Commun.*, vol. 20, no. 1, pp. 421–439, 2021.
- [60] J. Garcia, A. Sibille, and M. Kamoun, "Reconfigurable intelligent surfaces: Bridging the gap between scattering and reflection," *IEEE J. Sel. Areas Commun.*, vol. 38, no. 11, pp. 2538–2547, 2020.
- [61] S. Sugiura, C. Xu, S. X. Ng, and L. Hanzo, "Reduced-complexity iterative-detection-aided generalized space-time shift keying," *IEEE Trans. Veh. Technol.*, vol. 61, no. 8, pp. 3656–3664, 2012.
- [62] C. Xu, S. Sugiura, S. X. Ng, P. Zhang, L. Wang, and L. Hanzo, "Two decades of MIMO design tradeoffs and reduced-complexity MIMO detection in near-capacity systems," *IEEE Access*, vol. 5, pp. 18564–18632, 2017.
- [63] C. Xu, P. Zhang, R. Rajashekar, N. Ishikawa, S. Sugiura, Z. Wang, and L. Hanzo, "Near-perfect finite-cardinality generalized space-time shift keying," *IEEE J. Sel. Areas Commun.*, vol. 37, no. 9, pp. 2146–2164, 2019.
- [64] C. Xu, S. Sugiura, S. X. Ng, and L. Hanzo, "Spatial modulation and space-time shift keying: Optimal performance at a reduced detection complexity," *IEEE Trans. Commun.*, vol. 61, no. 1, pp. 206–216, 2013.
- [65] R. Rajashekar, K. Hari, and L. Hanzo, "Reduced-complexity ml detection and capacity-optimized training for spatial modulation systems," *IEEE Trans. Commun.*, vol. 62, no. 1, pp. 112–125, 2014.
- [66] C. Xu, T. Bai, J. Zhang, R. G. Maunder, S. Sugiura, Z. Wang, and L. Hanzo, "Constant-envelope space-time shift keying," *IEEE J. Sel. Topics Signal Process.*, vol. 13, no. 6, pp. 1387–1402, 2019.
- [67] A. Rezaei, A. Khalili, J. Jalali, H. Shafiei, and Q. Wu, "Energy-efficient resource allocation and antenna selection for IRS-assisted multicell downlink networks," *IEEE Wireless Commun. Lett.*, vol. 11, no. 6, pp. 1229–1233, 2022.
- [68] J. He, K. Yu, Y. Shi, Y. Zhou, W. Chen, and K. B. Letaief, "Reconfigurable intelligent surface assisted massive MIMO with antenna selection," *IEEE Trans. Wireless Commun.*, vol. 21, no. 7, pp. 4769–4783, 2022.
- [69] Z. Abdullah, G. Chen, S. Lambotharan, and J. A. Chambers, "Low-complexity antenna selection and discrete phase-shifts design in IRS-assisted multiuser massive MIMO networks," *IEEE Trans. Veh. Technol.*, vol. 71, pp. 3980–3994, 2022.
- [70] S. Zhang, S. Zhang, F. Gao, J. Ma, and O. A. Dobre, "Deep learning optimized sparse antenna activation for reconfigurable intelligent surface assisted communication," *IEEE Trans. Commun.*, vol. 69, no. 10, pp. 6691–6705, 2021.
- [71] Z. Wang, L. Liu, and S. Cui, "Channel estimation for intelligent reflecting-surface assisted multiuser communications: Framework, algorithms, and analysis," *IEEE Trans. Wireless Commun.*, vol. 19, no. 10, pp. 6607–6620, 2020.
- [72] T. L. Jensen and E. De Carvalho, "An optimal channel estimation scheme for intelligent reflecting surfaces based on a minimum variance unbiased estimator," in *IEEE Int. Conf. Acoustics, Speech Signal Process. (ICASSP)*, 2020.
- [73] Q. Nadeem, H. Alwazani, A. Kammoun, A. Chaaban, M. Debbah, and M. Alouini, "Intelligent reflecting surface-assisted multi-user MISO communication: Channel estimation and beamforming design," *IEEE Open J. the Commun. Society*, vol. 1, pp. 661–680, 2020.
- [74] R. Steele and L. Hanzo, *Mobile Radio Communications*. John Wiley & Sons, May 1999.
- [75] J. G. Proakis, *Digital Communications*. New York: McGraw-Hill, 1995.
- [76] A. Goldsmith, *Wireless communications*. Cambridge University Press, 2005.
- [77] L. Hanzo, O. Alamri, M. El-Hajjar, and N. Wu, *Near-Capacity Multi-Functional MIMO Systems: Sphere-Packing, Iterative Detection and Cooperation*. John Wiley & Sons, May 2009.
- [78] I. A. Hemadeh, K. Satyanarayana, M. El-Hajjar, and L. Hanzo, "Millimeter-wave communications: Physical channel models, design considerations, antenna constructions, and link-budget," *IEEE Commun. Surveys Tut.*, vol. 20, pp. 870–913, Secondquarter 2018.
- [79] T. S. Rappaport, Y. Xing, O. Kanhere, S. Ju, A. Madanayake, S. Mandal, A. Alkhateeb, and G. C. Trichopoulos, "Wireless communications and applications above 100 GHz: Opportunities and challenges for 6G and beyond," *IEEE Access*, 2019.
- [80] D. Divsalar and M. K. Simon, "Maximum-likelihood differential detection of uncoded and trellis coded amplitude phase modulation over AWGN and fading channels-metrics and performance," *IEEE Trans. Commun.*, vol. 42, pp. 76–89, 1994.
- [81] R. Schober and W. H. Gerstacker, "Decision-feedback differential detection based on linear prediction for MDPSK signals transmitted over Ricean fading channels," *IEEE J. Sel. Areas Commun.*, vol. 18, pp. 391–402, Mar. 2000.
- [82] T. Cui and C. Tellambura, "On multiple symbol detection for diagonal DUSTM over Ricean channels," *IEEE Trans. Wireless Commun.*, vol. 7, pp. 1146–1151, April 2008.
- [83] R. H. Clarke, "A statistical theory of mobile radio reception," *Bell Labs Technical Journal*, vol. 47, pp. 957–1000, 1968.
- [84] W. C. Jakes, *Microwave mobile communications*. John Wiley & Sons, 1975.
- [85] N. S. Perovic, L.-N. Tran, M. D. Renzo, and M. F. Flanagan, "Achievable rate optimization for MIMO systems with reconfigurable intelligent surfaces," *IEEE Trans. Wireless Commun.*, vol. 20, no. 6, pp. 3865–3882, 2021.
- [86] J. C. Chen, "Machine learning-inspired algorithmic framework for intelligent reflecting surface-assisted wireless systems," *IEEE Trans. Veh. Technol.*, vol. 70, no. 10, pp. 10671–10685, 2021.
- [87] P. Wang, J. Fang, H. Duan, and H. Li, "Compressed channel estimation for intelligent reflecting surface-assisted millimeter wave systems," *IEEE Signal Process. Lett.*, vol. 27, pp. 905–909, 2020.
- [88] X. Ma, Z. Chen, W. Chen, Z. Li, Y. Chi, C. Han, and S. Li, "Joint channel estimation and data rate maximization for intelligent reflecting surface assisted terahertz MIMO communication systems," *IEEE Access*, pp. 99565–99581, 2020.
- [89] J. An, C. Xu, L. Gan, and L. Hanzo, "Low-complexity channel estimation and passive beamforming for RIS-assisted MIMO systems relying on discrete phase shifts," *IEEE Trans. Commun.*, vol. 70, no. 2, pp. 1245–1260, 2022.

- [90] Z. He and X. Yuan, "Cascaded channel estimation for large intelligent metasurface assisted massive mimo," *IEEE Wireless Commun. Lett.*, vol. 9, no. 2, pp. 210–214, 2020.
- [91] H. Liu, X. Yuan, and Y. A. Zhang, "Matrix-calibration-based cascaded channel estimation for reconfigurable intelligent surface assisted multiuser MIMO," *IEEE J. Sel. Areas Commun.*, vol. 38, no. 11, pp. 2621–2636, 2020.
- [92] C. Xu, J. An, T. Bai, S. Sugiura, R. G. Maunder, Z. Wang, L. L. Yang, and L. Hanzo, "Channel estimation for reconfigurable intelligent surface assisted high-mobility wireless systems," *IEEE Trans. Veh. Technol.*, pp. 1–16, 2022.
- [93] C. Xu, J. An, T. Bai, L. Xiang, S. Sugiura, R. G. Maunder, L. L. Yang, and L. Hanzo, "Reconfigurable intelligent surface assisted multi-carrier wireless systems for doubly selective high-mobility rician channels," *IEEE Trans. Veh. Technol.*, vol. 71, no. 4, pp. 4023–4041, 2022.